Chemical Engineering Science 314 (2025) 121817

Contents lists available at ScienceDirect

Chemical Engineering Science

journal homepage: www.elsevier.com/locate/ces

# Modeling of radial heat transfer in cooled fixed-bed reactors by one- and two-dimensional models: Fischer-Tropsch synthesis as a case study

Christoph Kern, Andreas Jess *

*Chair of Chemical Engineering, Centre of Energy Technology, University of Bayreuth, Universitätsstraße 30, 95440 Bayreuth, Germany*

ARTICLE INFO

*Keywords:*
Fischer-Tropsch
Multi-tubular reactor
Heat transfer
1D and 2D model
Thermal runaway

ABSTRACT

New correlations for the overall heat transfer coefficient $U_{th}$, designed for use in one-dimensional reactor models for wall-cooled tubular fixed-bed reactors, are presented. These correlations are applicable for estimating both critical conditions related to thermal runaway and reactor performance under safe operating conditions. They were derived by comparing a 1D and a 2D model, initially for Fischer-Tropsch synthesis (FTS) as a case study, and subsequently extended beyond this specific reaction system. Additionally, a novel approach is introduced for estimating critical runaway conditions without relying on a reactor model. This method is based solely on reaction kinetics, the effective thermal conductivity $\lambda_{rad}$, and the heat transfer coefficient $\alpha_{wall}$, which accounts for heat transfer near the reactor wall.

## 1. Introduction

For Fischer-Tropsch synthesis (FTS), multi-tubular reactors are commonly employed to regulate reaction temperatures and ensure safe operation while minimizing the risk of thermal runaway. These reactors typically contain up to 10,000 tubes, each with a diameter of 2 to 5 cm, which are cooled by circulating boiling water around them.

The risk of thermal runaway necessitates the analysis of reactor behavior using computer simulations based on reliable mathematical models. These models must accurately predict temperature and concentration profiles across various operational parameters, such as tube diameter and cooling temperature. Two-dimensional pseudohomogeneous (2D) models are widely used to account for radial temperature gradients within the catalyst bed and are recommended for accurately predicting thermal runaway. In contrast, pseudohomogeneous one-dimensional (1D) models simplify all heat transport resistances into a single lumped parameter, the overall heat transfer coefficient $U_{th}$, which can limit their predictive accuracy (Sauerhöfer-Rodrigo et al., 2024; Sanchez-Lopez et al., 2017; Mendez et al., 2017, 2019b; Kern and Jess, 2009). Nevertheless, 2D models are significantly more complex compared to their 1D counterparts.

The one-dimensional model will therefore continue to be used for online computations and process control studies (Froment and Bischoff, 1990). 1D-models are also highly valuable to evaluate the dynamic behaviour of fixed-bed reactors, e.g. for Fischer-Tropsch (Mendez and Ancheyta, 2019a, 2020b; Mendez et al., 2022). The differential equations of an extended dynamic 1D-model, which is actually two-dimensional with axial coordinate $z$ and time $t$ as variables, can be solved with significantly less computational effort compared to a 2D-model (with radial coordinate $r$ as third variable). In this case, a reliable correlation for the overall heat transfer coefficient is also needed.

In previous studies, we developed a detailed 2D model for a wall-cooled FTS fixed-bed reactor using a cobalt-based catalyst (Kern and Jess, 2023a, 2023b, 2023c, 2024a, 2024b). This model is now utilized to compare the accuracy of 1D and 2D models for FTS and, subsequently, for wall-cooled fixed-bed reactors in general. The study primarily addresses two key questions:

- How well do the predictions of the 1D model align with those of the inherently more accurate 2D model?
- Which correlation for the overall heat transfer coefficient $U_{th}$ is valid in a 1D model to estimate the risk of runaway and the corresponding ignition temperature, while also providing reliable predictions of conversion and axial temperature profiles under non-critical conditions? To the best of our knowledge, this remains up to now an open question, as discussed in this work.

In this paper, we first analyze these questions using FTS as an example and then assess whether the findings can be generalized to other wall-cooled fixed-bed reactors. Specific aspects of FTS, such as cobalt-catalyzed reaction kinetics and details of heat transfer

* Corresponding author.
*E-mail address:* jess@uni-bayreuth.de (A. Jess).

https://doi.org/10.1016/j.ces.2025.121817
Received 19 February 2025; Received in revised form 5 May 2025; Accepted 7 May 2025
Available online 8 May 2025

**Nomenclature**

| | |
|---|---|
| $Ar$ | Arrhenius number of temperature sensitivity (Eq. (23)) |
| $Bi$ | Biot number, ratio of external to internal heat transfer (Eq. (11)) |
| $C_A$ | coefficient of catalytic activity (in this work 3 for 30 wt% Co) |
| $c_i$ | concentration of $i$ (gas phase; $i$ = CO, $H_2$, $H_2O$), mol $m^{-3}$ |
| $d_{tube}$ | (internal) tube diameter, m |
| $D_{rad}$ | radial dispersion coefficient, $m^2$ $s^{-1}$ |
| $E_A$ | (effective) activation energy, J $mol^{-1}$ |
| $K$ | heat transfer parameter (Eq. (10)) |
| $K_{ig}$ | heat transfer parameter valid for thermal runaway |
| $m_{cat}$ | mass of catalyst, kg |
| $N_{cool}$ | dimensionless number of cooling capacity (Eq. (28)) |
| $N_{ad}$ | dimensionless number accounting for adiabatic T-rise (Eq. (29)) |
| $\dot{n}_{CO}$ | molar flux of CO, mol $s^{-1}$ |
| $Pe_o$ | molecular Peclet number (=$u_s\ \rho_g\ c_p\ d_p\ /\lambda_g$) |
| $Pe_{crit}$ | critical Peclet number (= 8 $\lambda_{bed}/\lambda_g$) |
| $\dot{q}_N$ | normalized radial heat flux per area (Eq. (20)) |
| $\dot{Q}_N$ | normalized radial heat flux (Eq. (19)) |
| $r$ | radial coordinate/distance in fixed-bed, m |
| $z$ | axial coordinate in fixed-bed, m |
| $r_{m,CO,C2+}$ | intrinsic reaction rate of CO conversion to methane, $mol_{CO}$ $kg_{cat}^{-1}$ $s^{-1}$ |
| $r_{m,CO\ CH4}$ | intrinsic reaction rate of CO conversion to $C_{2+}$-HCs, $mol_{CO}$ $kg_{cat}^{-1}$ $s^{-1}$ |
| $r_{m,CO,H2O}$ | intrinsic rate of CO, if inhibition by steam is considered, $mol_{CO}$ $kg_{cat}^{-1}$ $s^{-1}$ |
| $r_{m,CO,eff}$ | effective reaction rate of CO conversion, $mol_{CO}$ $kg_{cat}^{-1}$ $s^{-1}$ |
| $r_{m,CO,Tcool}$ | effective rate of CO at $T_{cool}$ and the initial concentrations of CO and $H_2$, $mol_{CO}$ $kg_{cat}^{-1}$ $s^{-1}$ |
| $r_N$ | normalized reaction rate of CO conversion (Eq. (26)) |
| $r_{tube}$ | (internal) tube radius, m |
| $R_{bed}$ | thermal resistance of fixed-bed, $m^2$ K $W^{-1}$ |
| $R_{th}$ | overall thermal resistance (= $1/U_{th}$), $m^2$ K $W^{-1}$ |
| $R_{wall}$ | overall thermal resistance at internal wall, $m^2$ K $W^{-1}$ |
| $Re_p$ | Reynolds number related to particle diameter (=$u_s\ d_p/\nu_g$) |
| $T$ | temperature, K, °C |
| $T_{ax,max}$ | maximum axial temperature, K, °C |
| $T_{bed}$ | temperature, K, °C |
| $T_{cool}$ | cooling temperature, K, °C |
| $T_{ig}$ | critical cooling temperature to reach ignition (thermal runaway), K, °C |
| $T_{mean}$ | mean temperature in the bed (typically at $r = 0.7\ r_{tube}$), K, °C |
| $T_{max}$ | temperature at the tube center ($r = 0$), K, °C |
| $T_{safe}$ | safe cooling temperature with regard to ignition, here 5 K below $T_{ig}$ |
| $T_{wall,1}$ | temperature at the (internal) wall before T-jump, K, °C |
| $T_{wall,2}$ | temperature at the (internal) wall after T-jump, K, °C |
| $T_{cool}$ | cooling temperature, K, °C |
| $U_{th,1D}$ | overall heat transfer coefficient related to 1D model, W $m^{-2}$ $K^{-1}$ |
| $U_{th,2D}$ | overall heat transfer coefficient related to 2D model for $K$ = 8, W $m^{-2}$ $K^{-1}$ |
| $X_{CO}$ | conversion of CO |

*Greek letters*

| | |
|---|---|
| $\Delta_R H_i$ | enthalpy of reaction, $i$ = reaction of CO to methane or to $C_{2+}$-HCs, J $mol_{CO}^{-1}$ |
| $\Delta\dot{Q}_N$ | normalized rate of heat production in a small radial segment (Eq. (26)) |
| $\Delta T_{ad,FTS}$ | adiabatic rise in temperature for Fischer-Tropsch synthesis, K, °C |
| $\Delta T_{bed,2D}$ | difference between $T_{max}$ and $T_{wall,1}$, K, °C |
| $\Delta T_N$ | normalized temperature difference in bed (Eq. (23)), K, °C |
| $\Delta T_{ig,1D}$ | difference between $T_{mean}$ and $T_{wall,2}$ (thermal runaway/ignition), K, °C |
| $\Delta T_{total,\ 1D}$ | difference between $T_{mean}$ and $T_{wall,2} = T_{cool}$, K °C |
| $\Delta T_{\alpha,wall}$ | difference between $T_{wall,1}$ and $T_{wall,2}$, K, °C |
| $\eta_{pore}$ | pore effectiveness factor |

*Abbreviations*

| | |
|---|---|
| 1D | one-dimensional (model) |
| 2D | two one-dimensional (model) |
| $C_{2+}$ | hydrocarbons with two and more carbon atoms |
| (–$CH_2$-) | methylene group of a normal paraffin |
| FTS | Fischer-Tropsch synthesis |
| HC(s) | hydrocarbon(s) |
| ig | related to ignition (thermal runaway of reactor) |

parameters, are only briefly discussed, as the underlying rate equations and mass/heat transfer correlations have already been presented in previous publications (Kern and Jess, 2023a, 2023b, 2023c, 2024a, 2024b).

It should be also noted that we used the pseudo-homogeneous 2D and 1D model, where the effective parameters of heat transfer (radial effective conductivity in the fixed-bed, wall heat transfer coefficient) are well-known. In the open literature, more complicate heterogenous models, composed of two heat balances for the gas and solid phase coupled by heat exchange between the two phases, are also used. These models require more parameters and estimations for heat transfer, which may also cause convergence issues.

## 2. Methodology: Kinetics of FTS and multi-tubular FTS reactor models

### 2.1. Intrinsic and effective reaction kinetics of FTS

The primary reaction of FTS, which yields predominantly paraffinic $C_{2+}$-hydrocarbons, is as follows:

$$CO + 2\ H_2 \rightarrow (–CH_2\text{-}) + H_2O\ \Delta_R H^0_{CH2298} = -\ 152\ kJ\ mol^{-1} \quad (1)$$

For a reliable kinetic description of FTS, methane formation must be considered separately:

$$CO + 3\ H_2 \rightarrow CH_4 + H_2O\ \Delta_R H^0_{CH4298} = -\ 206\ kJ\ mol^{-1} \quad (2)$$

The intrinsic reaction rates for methane ($r_{m,CO,CH4}$) and $C_{2+}$-hydrocarbons ($r_{m,CO,C2+}$), as well as internal diffusion limitations, have been experimentally determined in previous studies using Pt promoted (0.03 wt% Pt for Co reduction) Co/γ-$Al_2O_3$ catalysts (Pöhlmann and Jess, 2016a, b, Pöhlmann et al. 2016, Rößler et al., 2018, Pöhlmann, 2017). Both rates follow Langmuir-Hinshelwood kinetics and reflect the influence of the concentrations of CO and $H_2$ on the reaction rate. Details on the kinetics both on cobalt and iron catalyst can be found in a recent review (Mendez and Ancheyta, 2020a).

Since $CO_2$ formation via the water–gas shift reaction is minimal for cobalt catalysts, the total intrinsic reaction rate can be expressed as the sum of these individual rates:

$$r_{m,CO} = -\frac{d\dot{n}_{CO}}{dm_{cat}} = C_A\left(r_{m,CO,CH_4} + r_{m,CO,C_{2+}}\right) \quad (3)$$

The activity coefficient $C_A$ reflects the cobalt content and intrinsic activity, with a baseline value of 1 for a catalyst containing 10 wt% Co. FTS catalysts typically contain up to 30 wt% Co ($C_a \approx 3$), a value assumed throughout this study.

Steam inhibition is also considered, as indicated by our experimental data (Kern and Jess, 2023c):

$$r_{m,CO,H_2O} = r_{m,CO}\left(1 - \frac{c_{H_2O}}{472\ \text{mol m}^{-3}}\right) \quad (4)$$

A steam concentration of $c_{H2O} = 120$ mol/m$^3$ – corresponding to a CO conversion of 40 % and a steam partial pressure of 5 bar (at 30 bar total pressure, with a syngas composition of 31 % CO and 69 % $H_2$) – reduces the reaction rate by 25 %.

Equations (3) and (4) describe only the intrinsic reaction rate. However, in millimeter-sized catalyst particles, pore diffusion limitations reduce the effective rate to mitigate excessive pressure drop. The effective rate, incorporating the pore effectiveness factor $\eta_{pore}$ (see details in (Kern and Jess, 2023a, b, c, 2024a), is given by:

$$r_{m,CO,eff} = \eta_{pore} r_{m,CO,H_2O} \quad (5)$$

The pore effectiveness factor $\eta_{pore}$ is highly temperature-dependent. For the assumed particle diameter $d_p$ of 3 mm, $\eta_{pore}$ decreases significantly above 180 °C, reaching a value of 0.2 at 240 °C for $C_a = 3$ (Kern and Jess, 2024a, b). The effective activation energy of $r_{m,CO,eff}$ is 74 kJ/mol, which is a critical parameter for characterizing temperature sensitivity. Within a typical operating range of 200 to 250 °C, the reaction rate doubles with an increase of 20 K.

### 2.2. 2D model of cooled multi-tubular fixed-bed FTS reactor

The Equations (6) and (7) represent the mass and heat balance for a differential tube section (d$z$):

$$\frac{d(c_i u_s)}{dz} = \varepsilon_{bed} D_{rad}\left(\frac{1}{r}\frac{dT}{dr} + \frac{d^2T}{dr^2}\right) + r_{m,CO,eff}\rho_{bed} \quad (6)$$

$$c_p c_g \frac{d(Tu_s)}{dz} = \lambda_{rad}\left(\frac{1}{r}\frac{dT}{dr} + \frac{d^2T}{dr^2}\right) - r_{m,CO,eff}\left(0.8\Delta_R H_{CH_2} + 0.2\,\Delta_R H_{CH_4}\right)\rho_{bed} \quad (7)$$

The term 0.8 $\Delta_R H_{CH2}$ + 0.2 $\Delta_R H_{CH4}$ in Eq. (7) represents the mean reaction enthalpy of – 163 kJ/mol$_{CO}$ according to the selectivity to methane of 20 %.

The radial heat flux in the fixed-bed ($\dot{q}$ in W/m$^2$) toward the tube wall is governed by a radial effective conductivity $\lambda_{rad}$, while the internal heat transfer coefficient $\alpha_{wall,int}$ accounts for heat transfer near the wall. At the internal wall ($d_{tube}$ as internal tube diameter), both heat fluxes must be equal:

$$\dot{q} = -\lambda_{rad}\left.\frac{dT}{dr}\right|_{r=0.5d_{tube}} = \alpha_{wall,int}\left(T_{wall,1}(r = 0.5d_{tube}) - T_{wall,2}\right) \quad (8)$$

In addition to the intrinsic and effective kinetics outlined above, our FTS reactor model incorporates several critical aspects, as detailed in previous studies (Kern and Jess, 2023a, b, c, 2024a, b):

- The radial heat flux from the catalyst bed to the tube wall depends on the effective thermal conductivity $\lambda_{rad}$ and the radial temperature gradient at the wall, as described in Eq. (8). The parameter $\lambda_{rad}$ characterizes heat transfer within the pseudo-homogeneous phase, which includes both the catalyst and the gas phase, as both contribute to radial heat transport. $\lambda_{rad}$ is usually much higher than the thermal conductivity of the bed without gas flow ($\lambda_{bed}$), here by a factor of 8 (see Tab. 1). Within the catalyst bed, the temperature decreases from a maximum value ($T_{max}$) at the tube center to the temperature at the internal tube wall, denoted as $T_{w,int,1}$.
- At the inner tube wall, the heat transfer coefficient $\alpha_{wall,int}$ accounts for heat transfer very close to the internal tube surface. Similar to $\lambda_{rad}$, it is determined using literature correlations, specifically for FTS as provided in (Kern and Jess, 2023c). In reality, variations in flow velocity and packing density (i.e., increased porosity) near the wall lead to a significant reduction in the effective thermal conductivity $\lambda_{rad}$ (Dixon et al., 2013; Winterberg et al., 2000; Tsotsas and Schlünder, 1990; Winterberg and Tsotsas, 2000). This effect can be interpreted as an additional thermal resistance occurring in a narrow region near the wall, approximately within one particle diameter (Winterberg et al., 2000). To account for this effect, it is common practice – also applied in this study – to assume a constant $\lambda_{rad}$ across the entire catalyst bed while incorporating all wall-induced increases in thermal resistance into the heat transfer coefficient $\alpha_{wall,int}$, as e.g. discussed in more detail by Bey and Eigenberger (2001) and Zenner et al. (2019). This approach is often referred to as the $\alpha_{wall}$-model, leading to a "jump" in temperature from $T_{wall,1}$ to $T_{wall,2}$, which does not physically exist but provides a reasonable approximation (Eq. (8)).
- An alternative approach to the $\alpha_{wall}$-model, though rarely applied up to now in reactor modeling, is the $\lambda_{rad}$ ($r$)-model (Vortmeyer and Haidegger, 1991; Winterberg et al., 2000). This method eliminates the artificial temperature jump at the wall by introducing a radial profile for $\lambda_{rad}$, which remains constant in the core region of the reactor but declines sharply near the wall. There is a continuing debate in the literature, whether the $\alpha_{wall}$-model or the $\lambda_{rad}$ ($r$)-model should be used. As stated by Bey and Eigenberger (2001), both approaches give similar results for most industrial applications. This is underlined by Winterberg et al. (2000). According to this publication, the $\alpha_{wall}$-model is adequate, if the molecular Peclet number $Pe_o = u_s \rho_g c_p d_p / \lambda_g$ exceeds a certain critical value $Pe_{crit} = 8\ \lambda_{bed}/\lambda_g$ with $\lambda_{bed}$ as thermal conductivity of the bed without fluid flow. For the conditions in this work (Table 1), $Pe_o$ is 350 and thus much larger than the value of 32 for $Pe_{crit}$. Hence, we have chosen to apply the classical $\alpha_{wall}$-model in this study, assuming a constant $\lambda_{rad}$ throughout the bed and using the coefficient $\alpha_{wall,int}$ to account for wall effects.
- Although our latest, more advanced FTS reactor model indicates that $\lambda_{rad}$ and $\alpha_{wall,int}$ exhibit a certain, albeit mostly minor, dependence on the axial position – primarily due to changes in gas velocity caused by pressure drop and the gradual reduction in total molar flow along the reactor length via the FTS reaction (Kern and Jess, 2023c) – we

**Table 1**
Heat transfer parameters, operational conditions, and chemical media data used to model the FT reactor (at 230 °C and 30 bar). (Details in Kern and Jess, 2023a, b,c, 2024a, b).

| | |
|---|---|
| Effective radial thermal conductivity $\lambda_{rad}$ (base case only) | 4 W m$^{-1}$ K$^{-1}$ |
| Thermal conductivity of bed without gas flow $\lambda_{bed}$ | 0.48 W m$^{-1}$ K$^{-1}$ |
| Internal heat transfer coefficient (bed to tube wall) $\alpha_{wall}$ (base case only) | 1000 W m$^{-2}$ K$^{-1}$ |
| Overall heat transfer coefficient of fixed-bed for $K = 8$ (Eq. (10)); $U_{th} = 1/R_{th}$ | 516 W m$^{-2}$ K$^{-1}$ |
| Length of reactor (single tube) $L_{tube}$ | 12 $m$ |
| Internal tube diameter $d_{tube}$ | 3 cm |
| Initial molar content of CO, $H_2$, and $CH_4$ | 20 %, 44 %, and 36 % |
| Initial superficial gas velocity $u_{s,\ z\ =\ 0}$ | 0.5 m s$^{-1}$ |
| Total pressure $p$ (reactor inlet) | 30 bar |
| Diameter of spherical catalyst particles $d_p$ | 3 mm |
| Bulk density of bed/catalyst $\rho_{bed}$ | 960 kg m$^{-3}$ |
| Porosity of fixed-bed $\varepsilon_{bed}$ | 0.4 |
| Heat capacity of gas mixture $c_p$ | 35 J mol$^{-1}$ K$^{-1}$ |
| Density of gas mixture $\rho_g$ | 730mol m$^{-3}$ |
| Thermal conductivity of gas mixture $\lambda_g$ | 0.12 W m$^{-1}$ K$^{-1}$ |
| Radial dispersion coefficient in fixed-bed $D_{rad}$ | · 10$^{-4}$ m$^2$ s$^{-1}$ |

have opted to use constant values for both. This deliberate simplification ensures that the focus remains on the fundamental comparison between 1D and 2D reactor models, both for FTS and more generally for wall-cooled fixed-bed reactors.

- o Heat is conductively transferred through the steel wall and subsequently to the boiling water. However, these two thermal resistances are relatively small and were therefore neglected, assuming $T_{w,int,2} = T_{cool}$. This assumption, along with the previously mentioned simplifications of constant $\lambda_{rad}$ and $\alpha_{wall}$, was deliberately made to focus exclusively on the interplay $\lambda_{rad}$ and $\alpha_{wall,int}$, the latter of which is hereafter referred to as $\alpha_{wall}$.
- o The adiabatic temperature rise in FTS can reach up to 2000 K when using pure CO and $H_2$ as syngas. However, to prevent thermal runaway, the permissible temperature increase is typically limited to 50 K, necessitating intensive cooling and small tubes. In this study, a tube diameter ($d_{tube}$) of 3 cm is employed.
- o Radial dispersion of mass is considered in this study; however, its impact on reactor performance is minimal.
- o Syngas recycling is not explicitly accounted for in this study. Instead, a syngas composition of 44 % $H_2$, 20 % CO, and 36 % $CH_4$ is assumed, which is representative of conditions that enable a high overall syngas conversion of 95 % with recycle (Kern and Jess, 2023b). Additionally, it ensures an identical conversion of $H_2$ and CO, corresponding to a methane selectivity of 20 %.
- o The differential equations (DEs) for mass and heat balances were solved using Presto Kinetics, a reliable solver for DEs (CiT GmbH, Rastede, Germany).

The heat transfer parameters and other data used to model the FT reactor are listed in Table 1.

### 2.3. 1D model of multi-tubular FTS reactor

A one-dimensional (1D) model is significantly less complex than a two-dimensional (2D) model and provides a convenient first insight into reactor behavior. It assumes that concentration and, more importantly, temperature gradients occur only in the axial direction. Consequently, an overall radial heat transfer coefficient, $U_{th}$, is required to represent the combined effects of heat conduction in the bed ($\lambda_{rad}$) and heat transfer at the internal wall ($\alpha_{wall}$). In a 1D model, the bed temperature – and thus the reaction temperature – is assumed to be radially uniform. This temperature is denoted as $T_{mean}$. Ideally, $T_{mean}$ should correspond to a representative value that accurately reflects the "real" mean temperature and reaction rate within the bed. The overall heat transfer from the bed to the cooling medium (e.g., boiling water in FTS) is then described by:

$$\dot{q} = U_{th}(T_{mean} - T_{cool}) \tag{9}$$

The overall thermal transmittance (also named overall heat transfer coefficient) $U_{th}$ of a fixed-bed reactor and its reciprocal, the total thermal resistance $R_{th}$, is based on weighting the relative importance of radial conductivity ($\lambda_{rad}$) and wall heat transfer coefficient ($\alpha_{wall}$):

$$U_{th} = \frac{1}{R_{th}} = \frac{1}{(R_{wall} + R_{bed})} = \left(\frac{1}{\alpha_{wall}} + \frac{d_{tube}}{\lambda_{rad} K}\right)^{-1} \tag{10}$$

The factor $K$ in Eq. (10) is a critical parameter for the reliability of 1D reactor models. Literature values vary, with most sources suggesting $K = 8$, though $K = 6.13$ (Crider and Foss, 1965), $K = 6.12$ (Westerink et al., 1990), or $K = 6$ (Li and Finlayson, 1977) are have also recommended. A correlation allowing $K$ to vary with $Bi$ (see Eq. (11) below) was given by Dixon (1996). His correlation, $K = 6\ (Bi + 4)/(Bi + 3)$ in the notation of this work, leads to $K = 6$ in the limit $Bi \to \infty$, and to $K = 8$ in the limit $Bi \to 0$. In this paper, a new approach is presented to determine $K$ not only based on the $Bi$ number, but also for different radial temperature differences in the fixed-bed and kinetic parameters such as the activation energy.

## 3. Simulation of FTS reactor by 1D and 2D reactor model

### 3.1. Influence of Bi number on the thermal behavior of a cooled multi-tubular FTS reactor

The ratio of $\alpha_{wall}$ to the conductive heat transfer parameter inside the bed ($d_{tube}/2\ \lambda_{rad}$) defines the Biot number:

$$Bi = \frac{\alpha_{wall} d_{tube}}{2\lambda_{rad}} \tag{11}$$

In this study, $Bi$ was varied over a wide range from 0.1 to 100 to analyze its fundamental influence on the thermal behavior of the reactor. However, practical Biot number values for wall-cooled reactors typically fall within a narrower range of 1 to 10 (Westerink et al., 1990).

For the analysis, the 2D model was initially used. Fig. 1 illustrates the impact of $Bi$ on temperatures and temperature differences in the catalyst bed and at the reactor wall for a cooling temperature of 210 °C and a constant overall heat transfer coefficient $U_{th}$ of 516 W m$^{-2}$ K$^{-1}$.

The individual values of $\alpha_{wall}$ and $\lambda_{rad}$ were determined using Equations (11) and (10), with $K = 8$ in Equation (10). The axial position for analysis was always set at the location of the axial maximum temperature, which occurs at approximately $z = 2$ m.

For low Bi numbers, the radial temperature difference in the bed ($\Delta T_{bed}$) is small, while the difference at the wall ($\Delta T_{wall}$) is high. Conversely, for high $Bi$ values, this relationship is reversed. In the base case for FTS ($Bi = 3.75$), the differences are $\Delta T_{bed} = T_{max} - T_{wall,1} = 9$ K and $\Delta T_{wall} = 5$ K.

For the 1D model, an initial assumption of $K = 8$ was used in Equation (10), as this is frequently recommended in the literature. This leads to an overall heat transfer coefficient of $U_{th} = 516$ W m$^{-2}$ K$^{-1}$. However, if a lower value is more appropriate (e.g., $K = 6$ K), $U_{th}$ decreases to 444 W m$^{-2}$ K$^{-1}$.

At the internal wall, the heat flux from the bed to the wall (W m$^{-2}$) equals the flux determined by $\alpha_{wall}$ and the temperature $\Delta T_{wall}$. Using Equation (8), the heat flux can be expressed as:

$$\dot{q} = \alpha_{wall}\left(T_{wall,1} - T_{wall,2}\right) = \frac{K\lambda_{rad}}{d_{tube}}\left(T_{mean} - T_{wall,1}\right) \text{ for r } = 0.5 d_{tube} \tag{12}$$

According to Eq. (12), the gradient in the bed d$T$/d$r$ at the wall equals the term $(T_{mean} - T_{wall,1})/(d_{tube}/8)$, if a value of 8 is used for $K$, and the gradient and thus the heat flux is smaller for $K < 8$.

In general, the overall radial temperature difference predicted by the

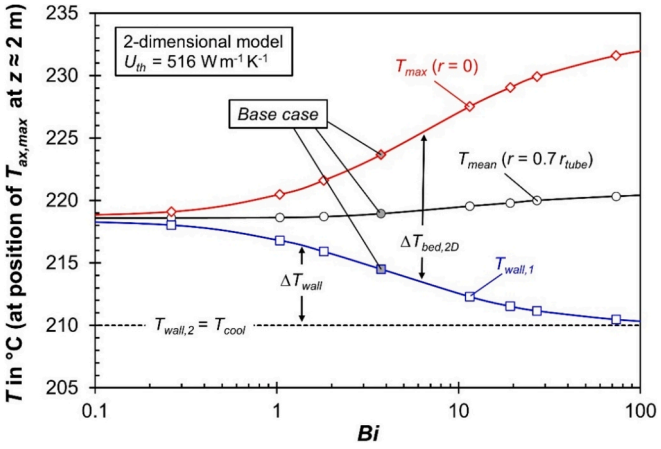


**Fig. 1.** Influence of $Bi$ number on $T_{max}$ (at $r = 0$), $T_{mean}$ ($r = 0.7\ r_{tube}$), and temperatures at internal wall ($T_{wall,1}$ and $T_{wall,2} = T_{cool}$) at the location of the axial temperature maximum for $U_{th}$ of 516 W m$^{-2}$ K$^{-1}$ and $K = 8$. Grey data points represent standard case of FTS with $Bi = 3.75$.

1D model is lower compared to the 2D model, since the 1D model assumes a radially uniform bed temperature $T_{mean}$:

$$\Delta T_{total,1D} = \left(T_{mean} - T_{wall,1}\right) + \left(T_{wall,1} - T_{wall,2}\right) = \frac{\Delta T_{bed,2D}}{2} + \Delta T_{wall} = \frac{1}{2}\left(\Delta T_{total,2D} + \Delta T_{wall}\right) \quad (13)$$

From Equations (12), (13), and (11), the relationship between $\Delta T_{bed,2D}$ and $\Delta T_{bed,1D}$ is derived as:

$$\Delta T_{bed,2D} = 2\Delta T_{bed,1D} = \Delta T_{total,1D}\frac{4Bi}{(K + 2Bi)} \quad (14)$$

For high *Bi* numbers, $\Delta T_{bed,2D} \approx 2\ \Delta T_{total,1D}$. In contrast, for low Bi numbers, $\Delta T_{bed,2D}$ is small, and the bed becomes nearly isothermal, making the 1D and 2D models almost identical (Fig. 1).

Fig. 2 shows the dependency of $\alpha_{wall}$ (heat transfer coefficient at wall) and heat conduction parameter 8 $\lambda_{rad}/d_{tube}$ (representing the bed resistance) for $U_{th}$ = 516 W m$^{-2}$ K$^{-1}$ and varying Biot numbers.

For the base case (*Bi* = 3.75), the values of $\alpha_{wall}$ (1000 W m$^{-2}$ K$^{-1}$) and 8 $\lambda_{rad}/d_{tube}$ (1067 W m$^{-2}$ K$^{-1}$) are nearly equal, demonstrating that heat transport in the bed and at the wall contribute approximately equally to the overall thermal resistance $R_{th}$.Results from the 2D model regarding the influence of the Biot number on CO conversion for different cooling temperatures are presented in Fig. 3 (left). Fig. 3 (right) illustrates the mean and maximum bed temperature as well as the wall temperatures for $T_{cool}$ = 220 °C in the 2D model.

For $T_{cool}$ = 220 °C and 225 °C, thermal runaway occurs when *Bi* exceeds a certain value, e.g., *Bi* = 25 for $T_{cool}$ = 220 °C. At first glance, this behavior appears unexpected, as $U_{th}$ remains constant. However, Fig. 2 demonstrates that at high Bi numbers, the overall heat transfer becomes increasingly limited by thermal conduction in the bed ($\lambda_{rad}$), leading to a stronger temperature sensitivity. It is crucial to emphasize that a 1D model only depends on the overall heat transfer coefficient $U_{th}$ (here 516 W m$^{-2}$ K$^{-1}$) and not on individual values of $\alpha_{wall}$ and $\lambda_{rad}$, and thus not on *Bi*. In contrast, 2D models explicitly consider *Bi*, making it a more accurate representation of reactor behavior.

Table 2 lists the CO conversion and characteristic radial temperatures at the location of the axial temperature maximum calculated by both the 1D- and 2D model for $T_{cool}$ = 210 and 220 °C. For the 2D-model, additional values for different *Bi* numbers are included. Fig. 4 depicts axial temperature profiles for both cooling temperatures and (for the 2D model) also for a high value of *Bi* of 19. For *Bi* < 1, the values of $T_{mean}$ and CO conversion remain nearly identical in both models. However, for high *Bi* values, the "true" values of $T_{mean}$ and conversion predicted by the 2D model are significantly higher than those of the 1D model. For example, at *Bi* = 19 and $T_{cool}$ = 220 °C, we get rounded values of:

- o 2D model: $T_{mean,2D}$ = 247 °C, $X_{CO,2D}$ is 74 %
- o 1D model: $T_{mean,1D}$ = 235 °C, $X_{CO,1D}$ of 68 %

For a lower $T_{cool}$ of 210 °C, the axial profiles of $T_{mean}$ are closely aligned for both models, even for *Bi* of 19. However, at $T_{cool}$ = 220 °C, where conditions approach ignition (220.4 °C), the deviation between the models becomes significant (upper part of Fig. 4). These results suggest that a constant factor of *K* = 8 should not be used in a 1D model when *Bi* numbers are high (> 10) or $T_{cool}$ approaches the critical ignition temperature. Under these conditions, the 1D model underestimates temperature and conversion, leading to inaccurate reactor predictions.

For *Bi* < 1, the mean bed temperature $T_{mean}$ (in Table 1 listed at position of axial maximum) and also the CO conversion do not depend on the model, but for a high value of *Bi,* the "true" value of $T_{mean}$ and the conversion deduced by the 2D model are considerably higher compared to 1D, as listed in Table 2 for *Bi* = 19. For a low cooling temperature of 210 °C, the axial profiles of $T_{mean}$ are closely together for both models, even for *Bi* of 19, but for $T_{cool}$ of 220 °C, already near ignition at 220.4 °C, the deviation is large (Fig. 4). This indicates that a constant factor *K* of 8 should not be used in a 1D model for high *Bi* numbers and if $T_{cool}$ approaches the ignition temperature.

### 3.2. Analysis of thermal runaway of a multi-tubular FTS reactor by 1D and 2D model

The runaway behavior of the FTS reactor was analyzed by varying the cooling temperature until thermal ignition occurred. In all cases, the position of the axial temperature maximum was considered. Fig. 5 (left) presents the results for the reliable 2D model, representing the "realistic" reactor behavior, and compares them to the 1D model for the case of *Bi* = 3.75. In the 1D model, two values for the parameter *K* were used, the standard value of 8 and a lower value of 6.2, for which the ignition temperature ($T_{ig}$) of the 1D model matches $T_{ig}$ of the 2D model at 226.5 °C. For *K* = 8, $T_{ig}$ is higher (231 °C), and the thermal sensitivity is significantly underestimated by the 1D model.

Fig. 5 (right) compares the CO conversion predicted by the 1D model for both values of *K* with the results from the 2D model: At low cooling temperatures, the 1D model with *K* = 8 closely approximates the "true" values from the 2D model. However, as runaway conditions are approached, the 1D model with *K* = 6.2 provides a better match to the 2D model, capturing the correct ignition temperature and reactor sensitivity.

Fig. 6 (left) presents the optimal values of *K* in the 1D model, ensuring that the mean bed temperature $T_{mean}$ predicted by the 1D model matches the "true" $T_{mean}$ of the 2D model (at the axial temperature maximum). The results indicate that *K* decreases from 8 to 6.2 as the cooling temperature $T_{cool}$ approaches the critical ignition temperature $T_{ig}$. With these adjusted *K*-values, the CO conversion obtained from the 1D and 2D models becomes nearly identical, with a deviation of less than 0.5 % (Fig. 6, right).

A similar study was conducted for a broad range of Biot numbers beyond the base case of *Bi* = 3.75. The results are illustrated in Figs. 7–9:

Fig. 7 demonstrates that by adjusting the ignition-related *K*-values ($K_{ig}$), the ignition temperature predicted by the 1D model closely aligns with the 2D model across different *Bi* numbers.

Fig. 8 (colored data) and Fig. 9 (left) validate the correlation $K_{ig}$ = f (*Bi*), confirming that it remains valid even when the overall thermal resistance $R_{th}$ (and $U_{th} = 1/R_{th}$) is varied significantly, from 0.5 to 2.5 times the base case of FTS ($R_{th,FTS}$ = 0.00194 m$^2$ K$^1$ W$^{-1}$).

As expected, Fig. 9 (right) illustrates that the ignition temperature $T_{ig}$ decreases with increasing $R_{th}$ (i.e. decreasing $U_{th}$), due to reduced cooling intensity. However, Fig. 9 (left) confirms that the optimal value $K_{ig}$ remains unaffected, further supporting the accuracy of the correlation presented in Fig. 8.

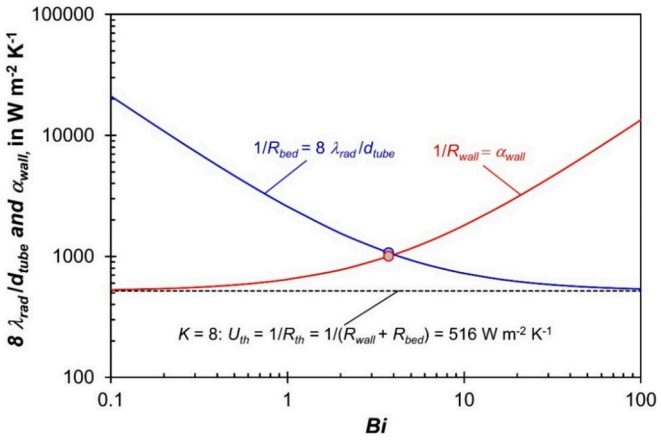


**Fig. 2.** Influence of *Bi* number on $\alpha_{wall}$ and heat conduction term 8 $\lambda_{rad}/d_{tube}$ for a constant $U_{th}$ and a value of 8 for *K*. The two data points represent standard case of FTS (*Bi* = 3.75).

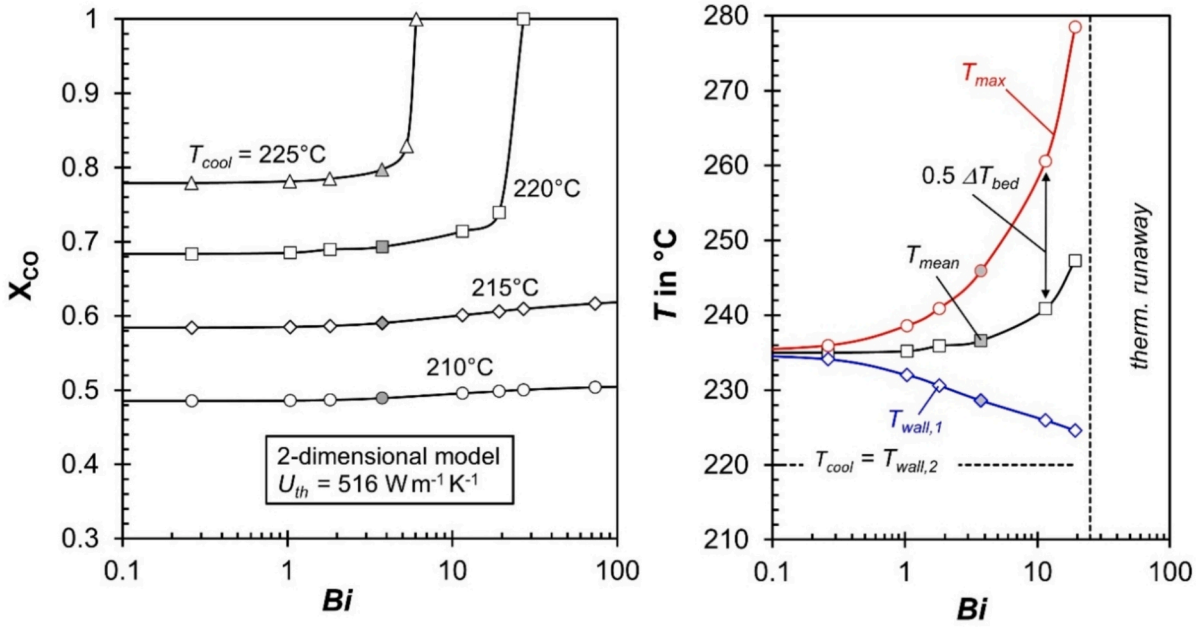


**Fig. 3.** Influence of *Bi* on reactor performance calculated by 2D model for $U_{th}$ of 516 W m$^{-2}$ K$^{-1}$ and $K = 8$. Left: CO conversion for different cooling temperatures. Right: $T_{max}$ (at $r = 0$), $T_{mean}$ ($r = 0.7\ r_{tube}$), $T_{wall,1}$ and $T_{wall,2} = T_{cool}$ at location of axial maximum, typically reached at $z = 2$ m. The grey data points represent standard case of $Bi = 3.75$.

**Table 2**
CO conversion and temperatures at location of maximum axial temperature (parameters in Tab. 1) calculated by a 1D- and 2D model for $T_{cool} = 210$ °C or 220 °C.

| | 1D-model | | 2D-model | | | | | | |
|---|---|---|---|---|---|---|---|---|---|
| $U_{th}$ in W m$^{-2}$ K$^{-1}$ | 516 | | | | | | | | |
| $\lambda_{rad}$ in W m$^{-1}$ K$^{-1}$ | only $U_{th}$ is needed (Eq. (10) with $K = 8$) | | 9.4 | 4 | 2.34 | 9.4 | 4 | 2.61 | 2.34 |
| $\alpha_{wall}$ in W m$^{-2}$ K$^{-1}$ | | | 650 | 1000 | 3000 | 650 | 1000 | 2000 | 3000 |
| *Bi*[a] | | | 1.04 | 3.75 | 19.2 | 1.04 | 3.75 | 11.5 | 19.2 |
| $T_{cool}$ in °C | 210 | 220 | 210 | | | 220 | | | |
| $T_{max}$ in °C | – | – | 220.5 | 223.7 | 229.0 | 238.6 | 245.9 | 260.6 | 278.5 |
| $T_{mean}$ in °C | 218.6 | 235.0 | 218.6 | 218.9 | 219.8 | 235.2 | 236.6 | 240.9 | 247.3 |
| $T_{wall,1}$ in °C | – | – | 216.8 | 214.5 | 211.5 | 232.0 | 228.6 | 225.2 | 223.7 |
| $X_{CO}$ | 48.5 % | 68.4 % | 48.6 % | 48.9 % | 49.8 % | 68.5 % | 69.3 % | 71.4 % | 74.0 % |

[a] *Bi* mainly depends on $Re_p$ ($=u_s\ d_p/\nu_g$). For the base conditions of FTS (Table 1), $u_s = 0.5$ m/s, $Re_p = 650$, and *Bi* is 3.75. For a 5 times lower/higher gas velocity, *Bi* would vary in a range of 2 to 6.

The value of *Bi* can vary between 2 and 6 for FTS (see footnote of Table 2). More generally, for wall-cooled reactors, $1 < Bi < 10$ is a typical range (Westerink et al., 1990). But this range is also where $K_{ig}$ exhibits a strong dependence on *Bi* (Figs. 8 and 9), further emphasizing the need to adjust *K* dynamically in 1D models when operating in this regime.

It should be noted that the values of $\alpha_{wall}$ and $\lambda_{rad}$ used in the 1D model were identical to those in the 2D model. This ensured that the ignition temperature $T_{ig}$ obtained in the 2D model (Fig. 7) corresponded to the "true" ignition temperature. The parameters $\alpha_{wall}$ and $\lambda_{rad}$ then lead by Eq. (10) and Eq. (11) to an overall heat transfer coefficient $U_{th,2D}$, in most cases in this work 516W m$^{-2}$ K$^{-1}$. To match the ignition temperature by the 1D model, a lower value of $U_{th,1D}$ was required. Based on this adjusted $U_{th,1D}$, the appropriate value of $K_{ig}$ was calculated, as shown in Fig. 8.

### 3.3. Radial heat transfer parameter K for s safe reactor operation beyond danger of runaway

Fig. 8 and Fig. 9 demonstrated that the ignition-related parameter $K_{ig}$ depends solely on the Bi number. This relationship remains valid beyond FTS, as further discussed in Section 4. For conditions below thermal runaway, i.e. for $T_{cool} < T_{ig}$, the temperature differences within the catalyst bed and at the wall decrease. This raises the question: Which value of *K* should be used in the 1D model to accurately describe heat transfer also under these subcritical conditions? Fig. 10 addresses this question by illustrating the influence of *Bi* on *K* in the FTS reactor. The values were chosen such that the 1D model reproduces the "real" mean bed temperature at the axial maximum, as obtained from the 2D model. However, since the 1D model assumes a uniform (mean) bed temperature, this temperature corresponds in the 2D model to the one at the radial position $r = 0.7\ r_{tube}$. The upper red dashed line in Fig. 10 represents the borderline case of thermal runaway, where $T_{cool} = T_{ig}$. The blue dashed line represents the correlation presented by Dixon (1996), as mentioned in the introduction.

For any value of *Bi*, *K* increases as $T_{cool}$ decreases. In Fig. 10, this trend is evident, and for low values of $T_{cool}$, *K* asymptotically approaches 8, at least for $Bi < 10$. For example, in the base case of FTS with $Bi = 3.75$: At ignition ($T_{cool} = 226.6$ °C), the lower limit of $K = 6$ is reached. For lower values of $T_{cool}$ we have: $T_{cool} = 220$ °C → $K = 7.1$, $T_{cool} = 210$ °C → $K = 7.5$, and $T_{cool} = 190$ °C → $K = 7.9$. This suggests that the appropriate *K*-value depends both on *Bi* and on the difference in bed temperature.

A lower *K*-value (e.g., 6 instead of 8) implies that the heat flux at the wall is reduced by 25 %. This observation may explain previous literature reports stating that experimentally determined values of $\lambda_{rad}$ and

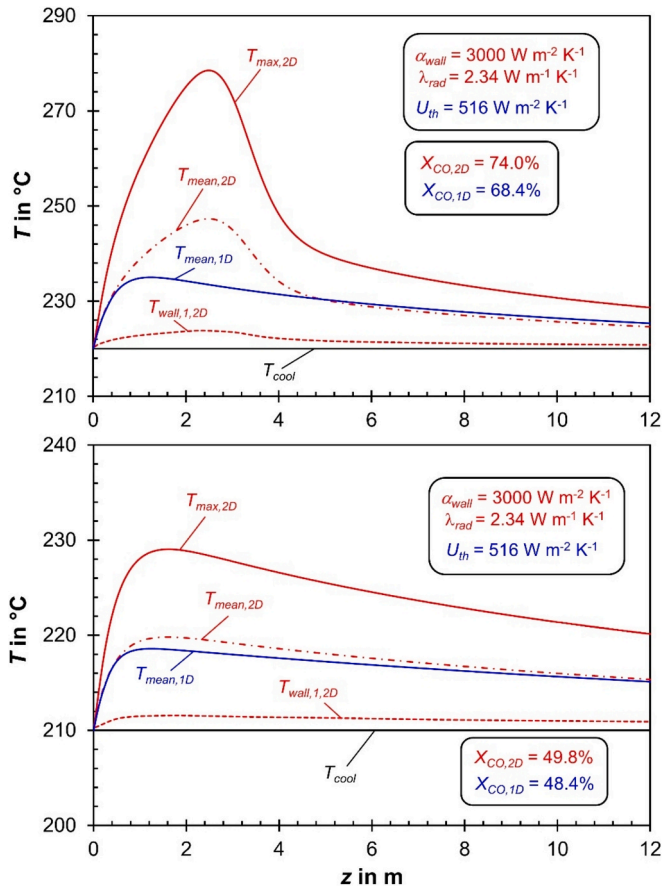


**Fig. 4.** Axial T-profiles calculated by the 1D- and 2D-model for $T_{cool}$ of 210 °C (bottom) and 220 °C (top). For the 2D-model (red), a high *Bi* number of 19 was assumed. For the 1D-model (blue), constant values of $U_{th}$ (516 W m$^{-2}$ K$^{-1}$) and of *K* (8) were used. The 1D model only delivers $T_{mean,1D}$ and not any information about the true radial temperature profile in the bed or about the assumed jump in temperature at the wall from $T_{wall1,2D}$ to $T_{wall,2,D2} = T_{cool}$.

$\alpha_{wall}$ under reaction conditions deviate significantly from those measured without reaction, up to 20 % lower for $\lambda_{rad}$ and even 50 % for $\alpha_{wall}$ for exothermic reactions as in case of FTS [Westerterp et al., 1998; Hofmann, 1979]. For endothermic reactions, Chao et al. (1973) have reported the reverse effect that heat transfer coefficients in packed beds under reacting conditions are always larger than those predicted by correlations obtained under non-reacting conditions. However, rather than being caused by an intrinsic change in $\lambda_{rad}$ and $\alpha_{wall}$ due to reaction effects, these deviations may simply reflect the change in *K* induced by the influence of reaction on the radial temperature profile, compared to non-reactive conditions. This hypothesis is further analyzed in the next sections.

The comparison of our results with the correlation of Dixon (Fig. 10) makes clear that Dixońs equation nicely reflects the same trend, but only represents fairly well mean values for a given number of *Bi*. As shown in Fig. 10 and analyzed in detail in the next section, *K* approaches the value of 8 even for relatively high *Bi* numbers, if the heat released by the reaction and thus the temperature difference in the fixed-bed is low. Conversely, *K* approaches the value of 5, if the heat released is high, e.g. for $Bi > 10$ and the case of thermal runaway. This is also not reflected by Dixońs correlation, $K = 6\ (Bi + 4)/(Bi + 3)$, which leads to a minimum value of $K = 6$ in the limit $Bi \rightarrow \infty$.

### 3.4. Radial temperature profiles in cooled fixed-bed reactors (example of FTS reactor)

The factor *K* in Eq. (10), as shown in Figs. 6, 8, and 9 for the onset of thermal runaway ($K_{ig}$) and in Fig. 10 for cases below ignition, has so far been determined purely by comparing the results of the 1D and 2D model. In this approach, the data obtained from the 2D model were considered the "truth," and the factors $K_{ig}$ and *K* in the 1D model were used solely as fitting parameters. It therefore remains an open question whether the correlation derived for $K_{ig}$ and *K*, as shown in Figs. 8 to 10, is only valid for FTS or whether it applies generally to cooled fixed-bed reactors.

To explore this, we begin with the simplifying assumption that the radial temperature profile in a cylindrical, wall-cooled packed bed with a chemical reaction maintains a parabolic curvature between tube

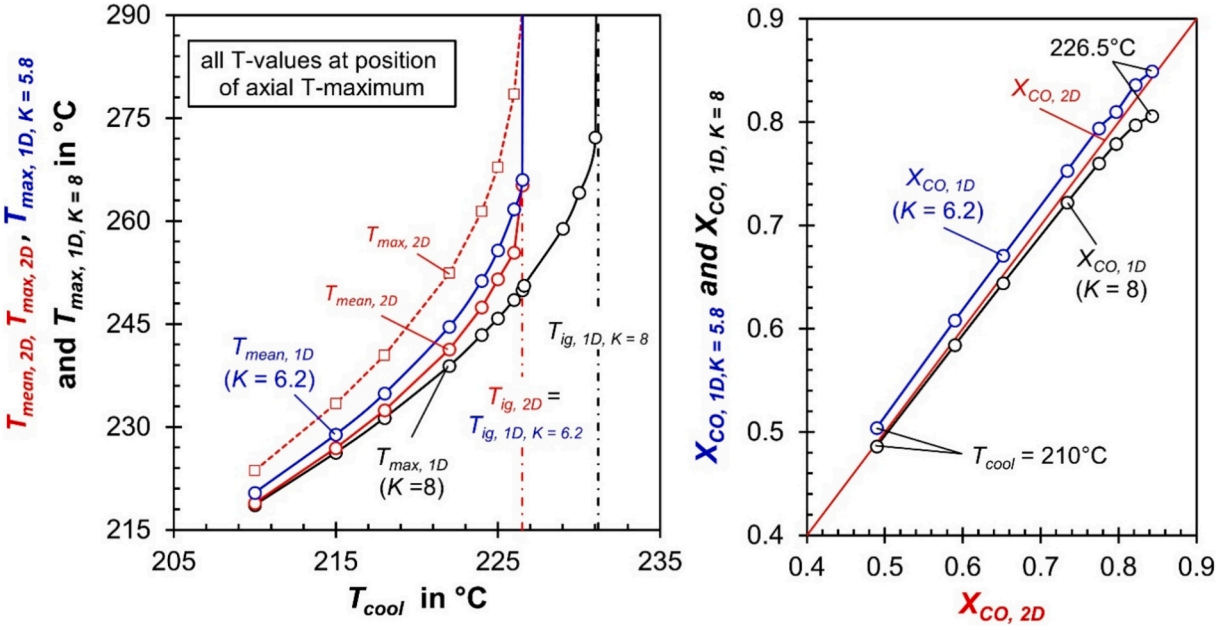


**Fig. 5.** Left: Influence of the $T_{cool}$ on $T_{max}$ in the tube center and $T_{mean}$ ($r \approx 0.7\ r_{tube}$) at the location of Fthe axial T-maximum according to 2D model (red data). For comparison, the results of the 1D-model for $U_{th}$ = 516 W m$^{-2}$ K$^{-1}$ ($K = 8$; black points) and 453 W m$^{-2}$ K$^{-1}$ ($K = 6.2$, blue points) are also shown. Right: CO conversion ($Bi = 3.75$; conditions in Tab. 1).

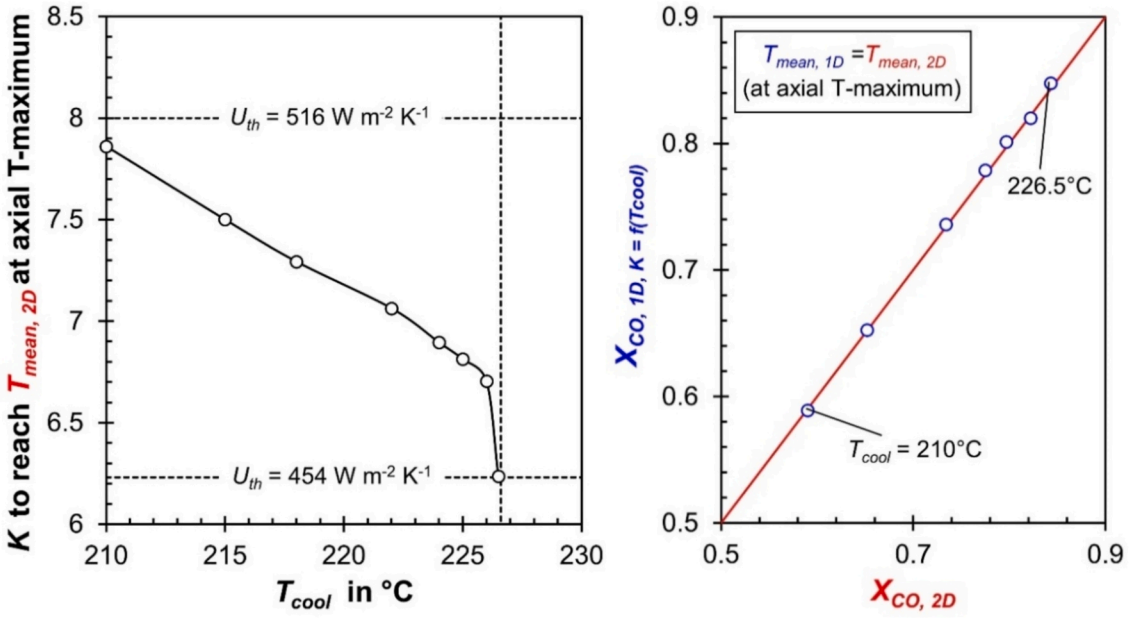


**Fig. 6.** Left: Influence of $T_{cool}$ on appropriate value of factor $K$ for 1D model to reach exactly the "true" value of $T_{mean}$ of 2D model at position of the maximum axial temperature (typically at $z$ = 1.5 m). Right: Comparison of CO conversion according to 1D model with $K$ as depicted left and true $X_{CO}$ of 2 D model ($Bi$ = 3.75; conditions in Tab. 1).

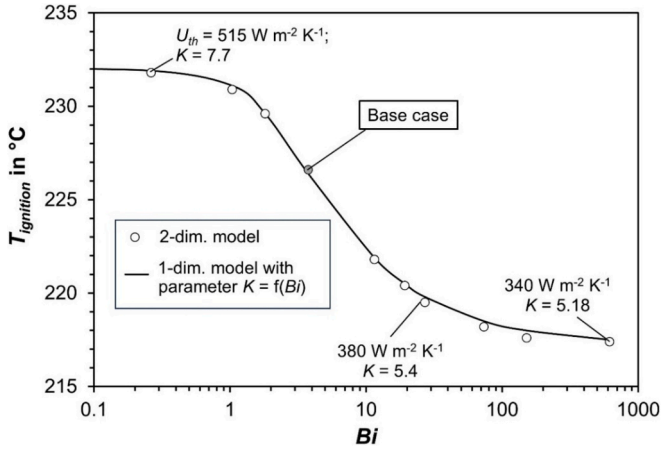


**Fig. 7.** Influence of $Bi$ on ignition temperature (onset of runaway) derived by the 2D model for $U_{th}$ of 516 W m$^{-2}$ K$^{-1}$ ($K$ = 8; Eq. (10)) and by the 1D model by appropriate values of the parameter $K$ (see Fig. 7) to match the "real" values of the 2D model.

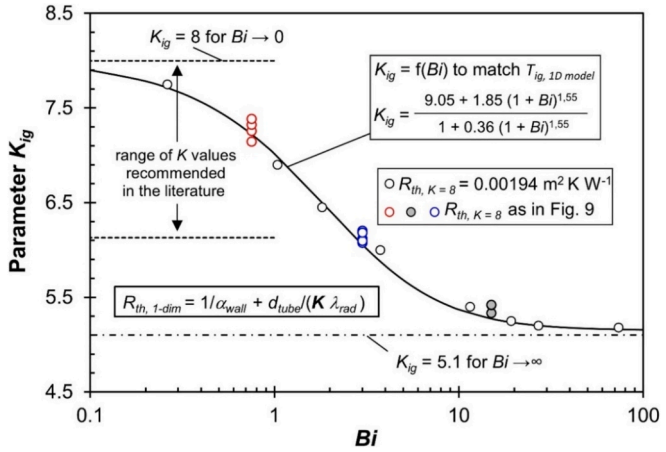


**Fig. 8.** Impact of $Bi$ on value of $K$ in 1D model to match the "real" values of $T_{ig}$ derived by 2D model (Fig. 6). (white symbols: $R_{th}$ for $K$ = 8 is 0.00194 m$^2$ K$^1$ W$^{-1}$, i.e. $U_{th,2D}$ = 516 W m$^{-2}$ K$^{-1}$; grey, red and blue symbols: $R_{th}$ for $K$ = 8 in a range 0.0009 to 0.0048 m$^2$ K$^1$ W$^{-1}$, i.e. $U_{th,2D}$ varies between 2000 and 200 W m$^{-2}$ K$^{-1}$).

center ($T_{max}$) and internal wall ($T_{wall,1}$). This assumption is supported by various experimental and numerical studies, including those by Emig and Klemm (2005), Westerterp et al., (1998), and Froment and Bischoff (1990). Accordingly, the temperature at any radial position is given by:

$$T_r = T_{wall,1} + \left(T_{max} - T_{wall,1}\right)\left[1 - 4\frac{r^2}{d_{tube}^2}\right] \tag{15}$$

To derive Eq. (15), a uniform heat production across the cross-section is assumed, which is, of course, not entirely valid. As discussed in Section 4, the parabolic curvature of the radial temperature profile, as described by Eq. (15), is only strictly applicable to a cylindrical geometry, if the reaction rate, and thus the heat release, are independent of temperature and/or if the temperature gradient within the bed is low. When there is a significant temperature difference in the bed, combined with a reaction rate that is highly sensitive to temperature (i.e., high activation energy), the profile flattens.

The mean temperature in the one-dimensional model corresponds to the temperature at the radial position $r_{mean}$ = 0.707 $r_{tube}$ = 0.354 $d_{tube}$ in the 2D model. This position divides the packed bed radially into two regions of equal volume. However, this assumption is strictly valid only if the activation energy and/or the temperature difference within the bed are low. Under these conditions, the mean radial temperature serves as a reasonable approximation for the entire cross-section.

It is essential to consider that the reaction rate varies significantly with temperature, making this purely geometrical approach not entirely exact. Nonetheless, it provides a convenient and widely used approximation. The mean temperature at $r_{mean}$ is given by:

$$T_{mean} = T_{max} - \frac{\left(T_{max} - T_{wall,1}\right)}{2} = \frac{\left(T_{max} + T_{wall,1}\right)}{2} \tag{16}$$

The heat flux from the bed to the wall corresponds to the derivative

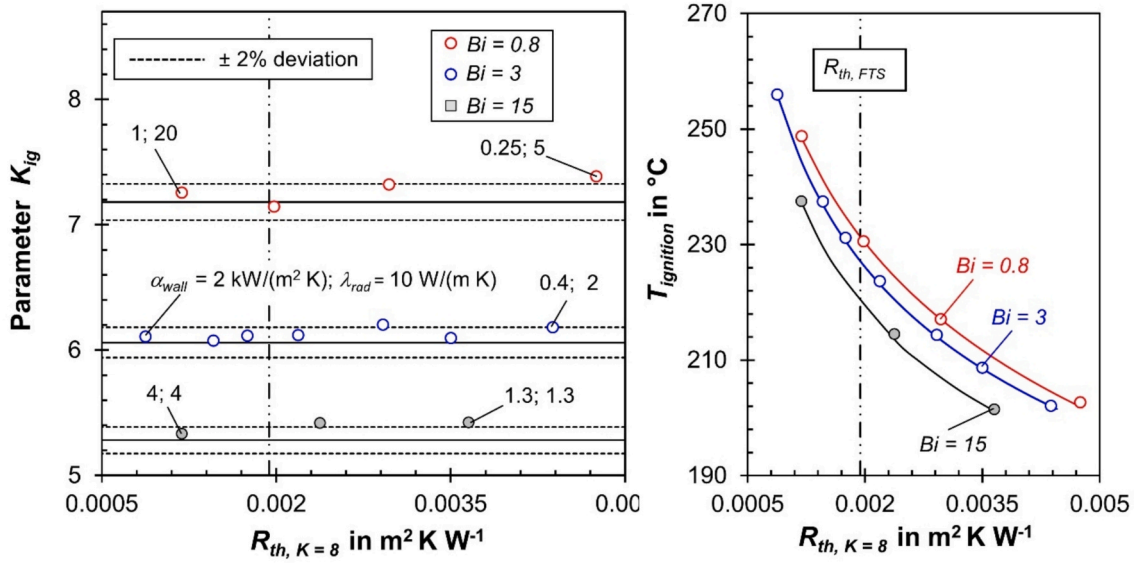


**Fig. 9.** Left: Influence of $R_{th}$ (= $1/U_{th}$) on appropriate value of $K_{ig}$ in the 1D model to match the "real" $T_{ig}$ derived by 2D model (Figs. 7 and 8) for 3 values of *Bi*. Right: Ignition temperatures.

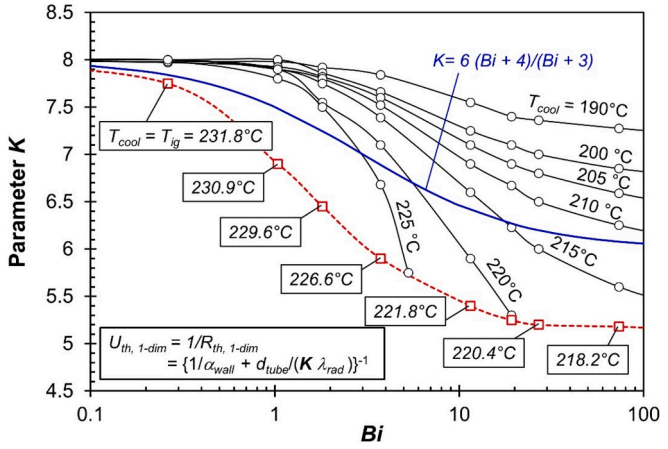


**Fig. 10.** Influence of Bi on value of K in 1D model of FTS reactor to match the "real" values of $T_{mean}$ of the 2D model at position of axial maximum in temperature. The 1D approach assumes a constant bed temperature, which corresponds to the value reached by the 2D model at r = 0.7 $r_{tube}$. The lower red dashed line represents case of runaway. The blue line represents the correlation presented by Dixon (1996).

of Eq. (15) evaluated directly at the internal wall of the reactor, i.e., at the radial position $r = 0.5\ d_{tube} = r_{tube}$. This results in:

$$\dot{q} = -\lambda_{rad}\left.\frac{dT}{dr}\right|_{r=r_{tube}} = \frac{8\lambda_{rad}}{d_{tube}}\left(T_{mean} - T_{wall,1}\right) \tag{17}$$

The derivation confirms that the factor $K = 8$ in Eq. (17) for the conductive heat transfer resistance within a packed bed is valid, provided that the parabolic curvature of the radial temperature profile remains unchanged by the reaction. However, various authors report different values for *K*, for example, Crider and Foss (1965) suggest $K = 6.12$ instead of 8. This lower value is particularly recommended for accurately predicting thermal runaway, as noted by Westerink et al. (1990). These findings align with the conclusions of this study, where *K* depends on *Bi* and may be lower than 8.

To gain a deeper understanding of why *K* depends on *Bi* and the magnitude of the temperature difference within a packed bed, it is useful to examine radial temperature profiles derived from the 2D model. Figs. 11 and 12, using FTS as example, illustrate that the parabolic shape of the radial profile from Eq. (15) does not hold when the temperature difference in the bed is large.

Fig. 11 (right) demonstrates that for an extremely high heat transfer coefficient at the wall (high *Bi*) – and consequently a strong temperature gradient within the bed – the radial temperature profile flattens significantly compared to the parabolic shape. This flattening reduces the radial temperature gradient at the wall, leading to a lower radial heat flux and, consequently, a lower *K*-value compared to the standard $K = 8$. This effect is particularly pronounced near ignition and at high *Bi* values, as shown in Fig. 12 (right). In contrast, for low *Bi* values, the parabolic temperature profile remains nearly valid, as seen in Fig. 11 (right, blue line) and Fig. 12 (left). Although the *Bi* values chosen in Figs. 11 and 12 deviates from realistic FTS conditions – where $Bi = 3.75$ under the conditions in Table 1 and practical values typically fall within $1 < Bi < 10$ (Westerink et al., 1990) – the extreme values of $Bi = 0.26$ and 605 in Fig. 11 and even $Bi = 0.014$ in Fig. 12 were intentionally chosen to clearly illustrate the strong parabolic curvature at low *Bi* and the profile flattening at high *Bi*.

It is evident that large radial temperature differences significantly alter the temperature profile due to the chemical reaction, which, in turn, leads to a radial variation in the reaction rate. This variation is governed by the activation energy – for FTS, $E_A = 74$ kJ/mol. In Section 4, the impact of the rate on the temperature profile will be systematically analyzed, first for FTS and then for other processes.

## 4. General correlation for the radial heat transfer parameter *K* useful for 1D models

### 4.1. Impact of activation energy and radial temperature difference on the radial conductive heat transport within a wall cooled fixed-bed reactor

The (normalized) heat release by the chemical reaction in a small radial segment *i* of a wall-cooled fixed-bed with thickness $\Delta r$ and total number of segments $N_s$ is given as follows. The index *i* represents the radial segment number, where $i = 1$ at $r = 0$ (tube center) and $i = N_s = r_{tube}/\Delta r$ at $r = r_{tube}$ (internal wall of reactor tubes). The heat release depends on the local reaction rate $r_{m,r}$ at position r and is normalized to the maximum reaction rate $r_{m,max}$ occurring at $T_{max}$ in the tube center ($r = 0$):

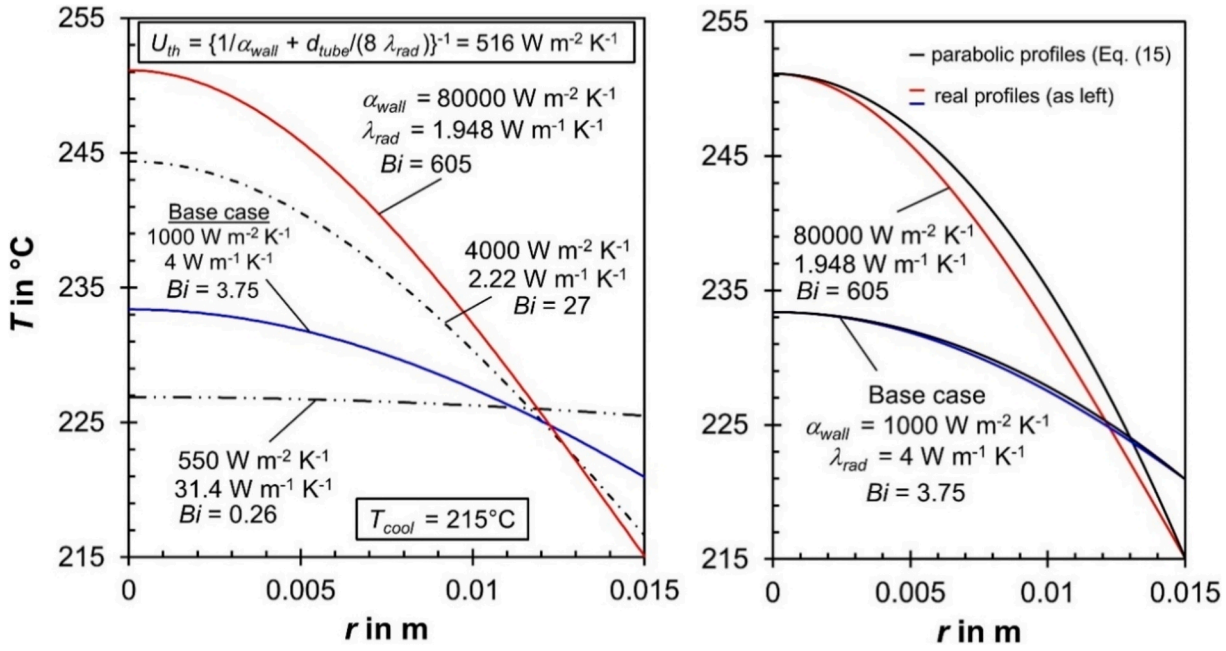


**Fig. 11.** Left: Radial T-profiles calculated by 2D model at position of axial T-maximum for different combinations of $\lambda_{rad}$ and $\alpha_{wall}$ (and thus *Bi*) for a constant $U_{th,2D}$. Right: Comparison of modelled profiles (red and blue curve) and parabolic profiles (black) according to Eq. (15), i.e. without influence of reaction and activation energy, for a high value of *Bi* (605) and the base case of FTS (*Bi* = 3.75).

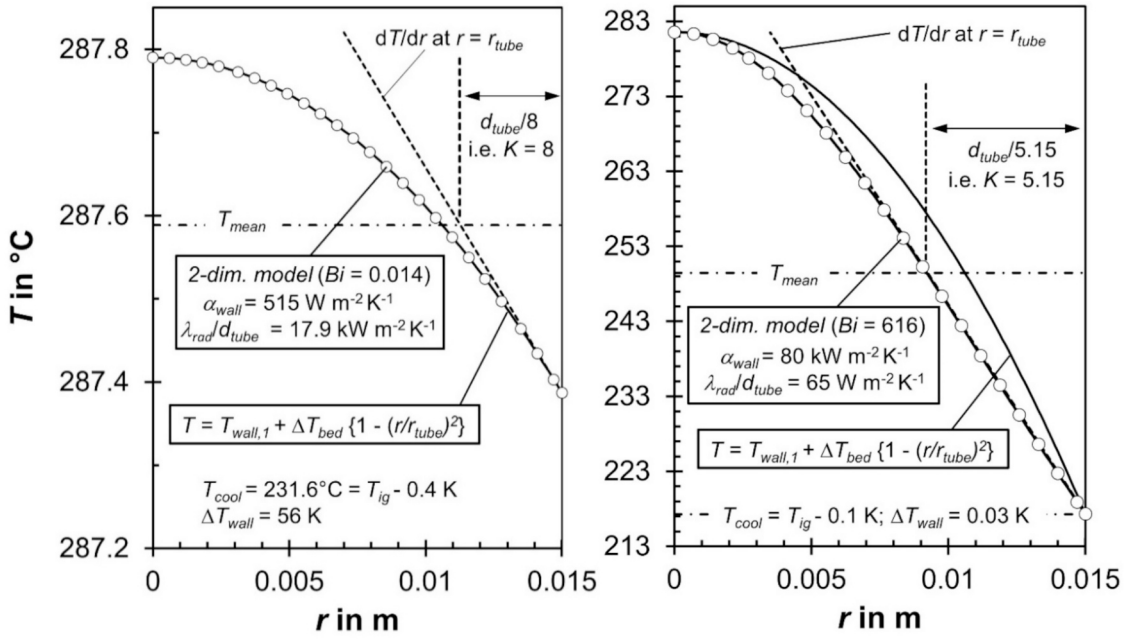


**Fig. 12.** Radial temperature profiles calculated by the 2D model for FTS for a very low (left) and a very high (right) value of the *Bi* number for $U_{th}$ (for $K = 8$) of 516 W m$^{-2}$ K$^{-1}$.

$$\Delta\dot{Q}_{N,i} = \frac{\Delta\dot{Q}_i}{\Delta\dot{Q}_{N_s}} = \frac{r_{m,r}}{r_{m,max}} \frac{2\pi r \Delta r L_{tube}}{2\pi r_{tube} \Delta r L_{tube}} = e^{-\frac{E_A}{R}\left(\frac{1}{T_r}-\frac{1}{T_{max}}\right)} \frac{r}{r_{tube}} = r_N \frac{r}{r_{tube}} \quad (18)$$

This expression provides insight into the spatial distribution of heat release within the radial profile of the reactor. The normalized reaction rate factor $r_N$ is 1 at $r = 0$ (tube center) and decreases toward the wall, reaching its minimum at $r = r_{tube}$. This behavior is illustrated in Fig. 13 (top) for an arbitrary example based on FTS with an activation energy $E_A$ = 74 kJ/mol and a relatively high temperature difference of 55 K within the bed, a condition close to thermal ignition.

The corresponding normalized radial heat flux is given by

$$\dot{Q}_{N,i} = \frac{\sum_1^i \Delta\dot{Q}_i}{\sum_1^{N_s} \Delta\dot{Q}_i} \quad (19)$$

as shown in Fig. 13 (bottom). This profile reflects the temperature gradient in the bed, with the maximum heat flux occurring near the tube wall, where the steepest gradient is present. Strictly speaking this expression is only valid at the axial position of the temperature maximum ($dT/dz = 0$), meaning that no heat is consumed or released to heat up or cool down the gas in the axial direction.

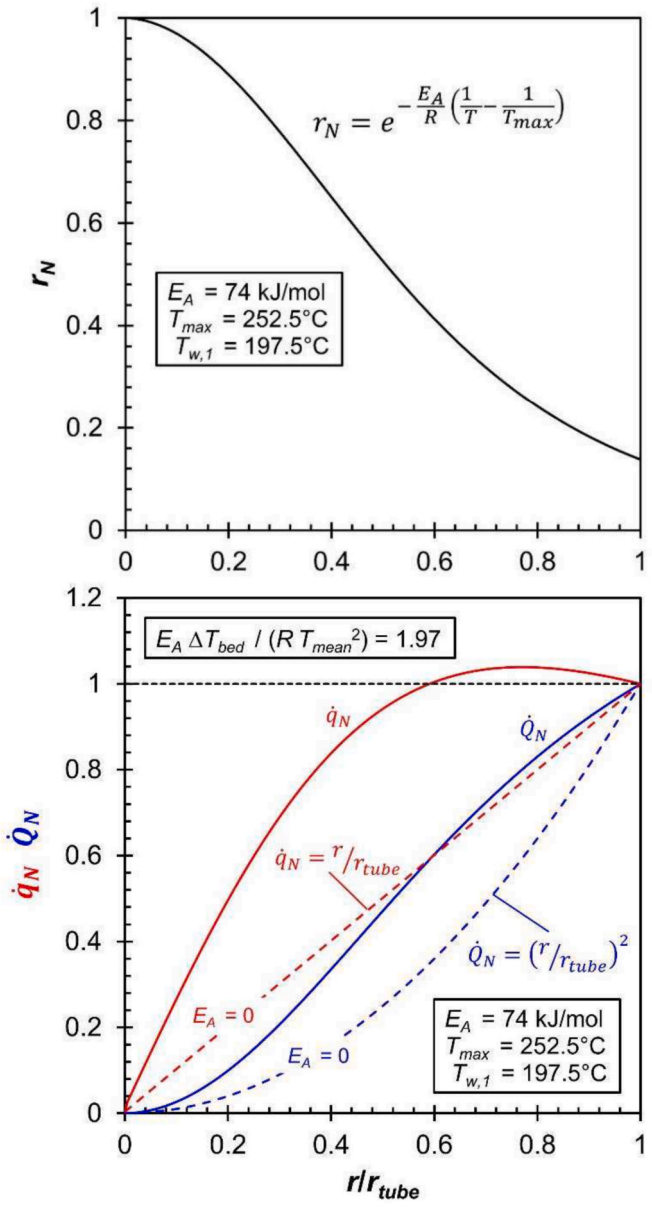


**Fig. 13.** Radial profiles of the dimensionless parameters $r_N$, $\dot{Q}_N$, and $\dot{q}_N$ for $E_A$ = 74 kJ/mol, $T_{max}$ = 252.5 °C, and $T_{wall,m1}$ = 197.5 °C. The radial T-profile is shown in the bottom of Fig. 14. Dashed lines (bottom) represent case of $r_N = 1$, i.e. $E_A = 0$, and are shown for comparison.

Based on Eq. (19), the normalized heat flux per area, shown in the bottom of Fig. 13, is given by:

$$\dot{q}_{N,i} = \frac{\dot{Q}_N}{r/r_{tube}} \tag{20}$$

This equation represents the radial heat flux profile, normalized to its maximum conductivity value, providing insight into the radial distribution of heat transfer in the bed. For comparison, the dashed lines in the bottom part of Fig. 13 show $\dot{Q}_N$ and $\dot{q}_N$ for $r_N = 1$, i.e. for $E_A = 0$ and hence the case of no influence of the reaction on the radial temperature profile. In this case, $\dot{Q}_N = (r/r_{tube})^2$ and $\dot{q}_N = r/r_{tube}$.

For any temperature difference in the bed, $\Delta T_{bed} = T_{max} - T_{min}$, the value in each radial segment $i$ is:

$$\Delta T_i = \frac{\dot{q}_{N,i}}{\sum_1^{N_s} \dot{q}_{N,i}} \Delta T_{bed} \tag{21}$$

Hence, the radial temperature profile is determined by:

$$T_r = T_{max} - \sum_1^i \Delta T_i \tag{22}$$

Since the actual radial temperature profile is a priori unknown, the parabolic profile from Eq. (15) was used as a starting point, assuming no influence of activation energy ($r_N = 1$). The actual profile was then derived iteratively, and is shown in the bottom of Fig. 14 for the example outlined in Fig. 13 with a high difference in bed temperature of 55 K as instructive example. Fig. 14 (middle and upper part) presents examples for two other radial temperature differences in the bed, 30 K and only 10 K, also assuming an activation energy of 74 kJ/mol, as in FTS. The results in Fig. 14 clearly show that the temperature gradient at the wall decreases with increasing temperature difference in the bed. Consequently, the factor $K$ decreases, from $K = 7.25$ for $\Delta T_{bed} = 10$ K to $K = 5.1$ for 55 K. In conclusion, a larger radial temperature difference in the bed leads to a lower radial heat flux, which in turn results in a lower

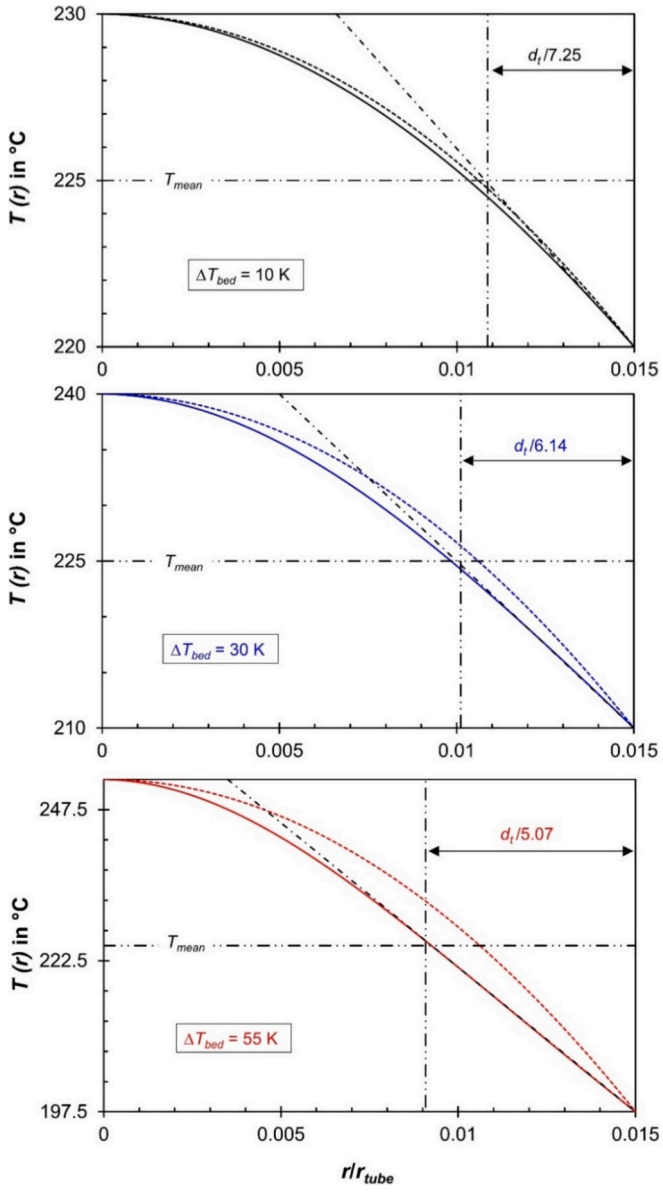


**Fig. 14.** Radial T-profiles calculated by 2D model for T-differences from 10 to 55 K in the bed and an activation energy of 74 kJ/mol (FTS). Comparison of (modelled profiles (full lines) and parabolic profiles (dotted lines) according to Eq. (15), i.e. without influence of reaction.

value of $K$.

Insertion: In this work, only cooled reactors and exothermic processes, such as FTS, are discussed. Applying Equations (18) to (22) to endothermic reactions would result in a steeper temperature gradient at the wall due to the influence of the chemical reaction, leading to an increased heat flux. Consequently, $K$ would be greater than 8, and $U_{th}$ would exceed the value calculated using Eq. (10) with $K \leq 8$. As mentioned in Section 3.3, this effect was confirmed by Chao et al. (1973), who observed higher heat transfer coefficients in heated packed beds under reacting conditions for the case of endothermic methane-steam reforming. However, this specific aspect related to endothermic processes is not further discussed in this study.

The correlation for $K$, derived from numerous modeling results, is presented in Fig. 15 for FTS at a mean temperature of 225 °C with an activation energy of $E_A = 74$ kJ/mol. Additionally, Fig. 16 extends this analysis to a broad range from 2 to 350 kJ/mol, and considers also extreme values of $T_{mean}$ at 8 °C and 1220 °C. The resulting correlation for $K$ is:

$$K = 8 - 1.72\left(\frac{E_A}{RT_{mean}}\frac{\Delta T_{bed,2D}}{T_{mean}}\right)^{0.8} = 8 - 1.72(Ar\Delta T_N)^{0.8} \quad (23)$$

In Eq. (23), the $Ar$ represents the Arrhenius number, defined as $Ar = E_A/(R\ T_{mean})$ where $E_A$ is the activation energy, $R$ is the universal gas constant, and $T_{mean}$ the mean bed temperature. The Arrhenius number serves as a measure of the temperature sensitivity of a reaction, which increases with higher activation energy, but is damped to some extent by a higher reaction temperature $T_{mean}$. The term $\Delta T_N$ is the normalized temperature difference in the bed, calculated from the 2D model as $\Delta T_N = \Delta T_{bed,2D}/T_{mean}$. This parameter is also significant: for low $\Delta T_N$, the radial temperature profile closely follows the parabolic profile predicted by Eq. (15), and the factor $K$ approaches 8.

The correlation for $K$ in Eq. (23) is particularly valuable for 1D models, as it allows for the determination of the appropriate $K$-value – and thus of $U_{th}$ via Eq. (10) – even for cases below ignition. Some iteration may be required, since the 1D model only determines $T_{mean}$ and, therefore, only the total temperature difference $\Delta T_{total,1D} = T_{mean} - T_{cool}$. However, the required $\Delta T_{bed,2D}$ and $\Delta T_N$, respecttively, needed for determining $K$ via Fig. 16 or Eq. (23) can be easily calculated using Eq. (14).

For the special case of runaway, where the maximum temperature difference between the mean bed temperature $T_{mean}$ and the cooling temperature $T_{cool} = T_{wall,2} - T_{wall,2}$ is reached, Eq. (14) yields:

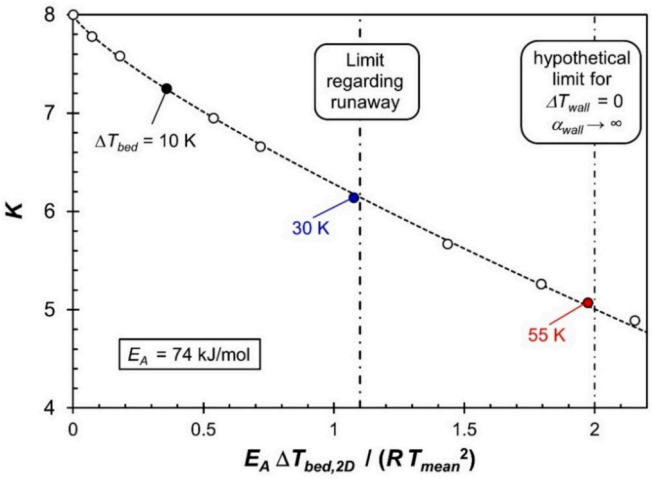


**Fig. 15.** Influence of term $E_A\ \Delta T_{bed,2D}/(R\ T_{mean}^2) = Ar\ \Delta T_N$ on parameter $K$ for an activation energy of 74 kJ/mol and a mean temperature of 225 °C, i.e. for typical conditions of FTS.

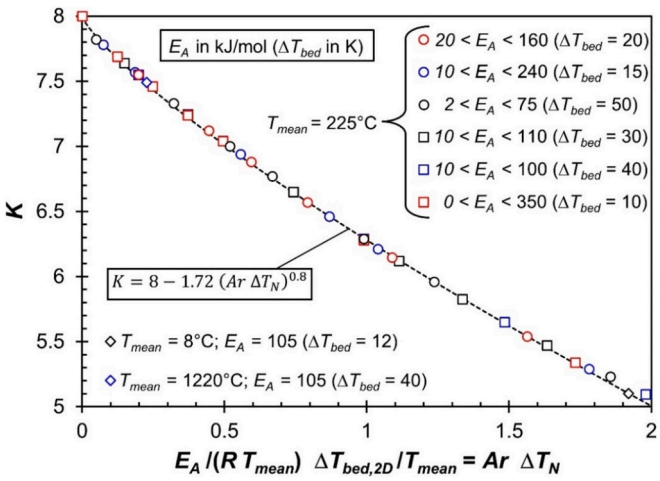


**Fig. 16.** Influence of term $Ar\ \Delta T_N$ on parameter $K$ for different activation energies, mean temperatures, and temperature differences in a cooled fixed-bed as indicated in the figure.

$$\frac{\Delta T_{bed,2D}}{\Delta T_{ig,1D}} = \frac{4Bi}{(K + 2Bi)} \quad (24)$$

$\Delta T_{ig,1D}$ can be estimated using a simple yet valuable formula for the maximum allowable temperature difference between the mean reaction temperature and the cooling temperature to prevent thermal runaway in a cooled fixed-bed reactor:

$$\Delta T_{ig,1D} \approx \frac{RT_{mean}^2}{E_A} \quad (25)$$

This expression provides a practical guideline for predicting critical operating limits, ensuring that the reactor remains within the safe operating range without exceeding the ignition threshold. This stability criterion was originally derived by Wilson in 1946 based on steady-state equations and later applied by Barkelew (1959) in his well-known work on the stability of chemical reactors. The temperature difference $\Delta T_{ig,1D}$ represents the maximum permissible increase in temperature before small fluctuations lead to an uncontrolled temperature rise (thermal runaway).

The maximum value of $Ar\ \Delta T_N$, as shown in Figs. 15 and 16, is 2, meaning that critical conditions are reached and runaway is inevitable. When $Ar\ \Delta T_N = 2$, the bed temperature difference in the 2D model satisfies the relation $\Delta T_{bed,2D} = 2\ \Delta T_{ig,1D}$ (Eq. (25)). Consequently, the temperature difference in the 1D model, $\Delta T_{bed,1D} = T_{mean} - T_{cool}$, already reaches $\Delta T_{ig,1D}$, meaning that even when the temperature difference at the wall is negligible (high $Bi$), runaway still occurs.

For $Bi < 10$, the contribution of $\Delta T_{wall}$ to $\Delta T_{total}$ is no longer negligible, as shown in Fig. 17 (right), so the critical value of $Ar\ \Delta T_N$ needed for ignition is lower than 2. In the base case of FTS with $Bi = 3.75$, ignition already occurs at $Ar\ \Delta T_N = 1.1$, where $\Delta T_{total} = 28$ K, the critical value according to Eq. (25). When ignition is reached, the relationship derived from Eq. (23) and Eq. (25) is:

$$K_{ig} = 8 - 1.72\left(\frac{\Delta T_{bed,2D}}{\Delta T_{ig,1D}}\right)^{0.8} \Rightarrow \frac{\Delta T_{bed,2D}}{\Delta T_{ig,1D}} = \left(\frac{8 - K_{ig}}{1.72}\right)^{1.25} \quad (26)$$

Insertion of Eq. (23) into Eq. (26) leads to the reversal function for $K_{ig} = f(Bi)$, i.e. to $Bi = f(K_{ig})$:

$$\frac{4Bi}{(K_{ig} + 2Bi)} = \left(\frac{8 - K_{ig}}{1.72}\right)^{1.25} \Rightarrow Bi = \frac{K_{ig}}{\left\{4\left(\frac{1.72}{8-K}\right)^{1.25} - 2\right\}} \left(8 < K_{ig} < 5.005\right) \quad (27)$$

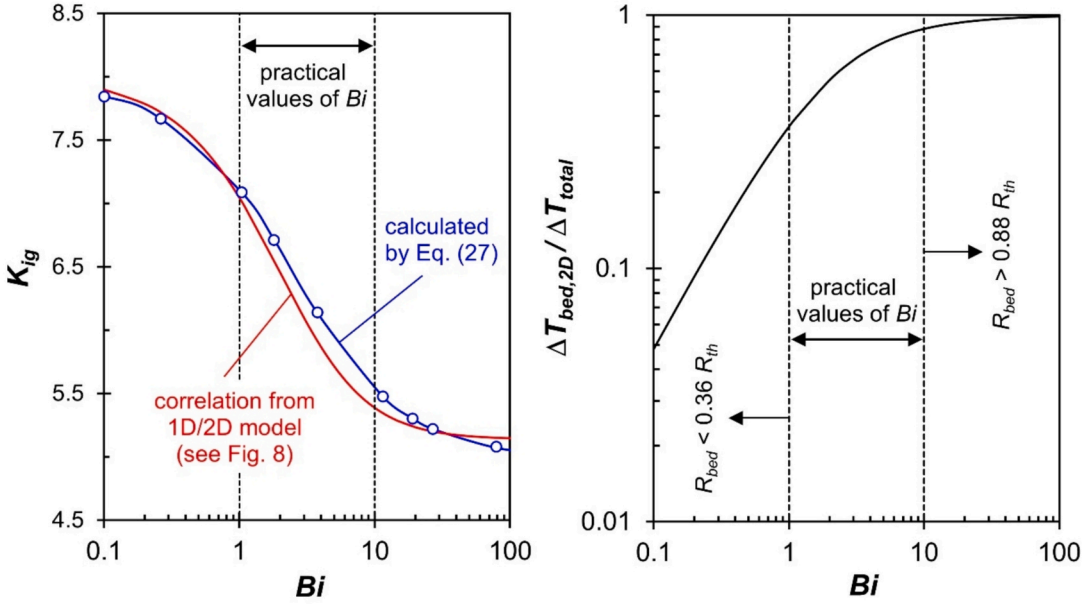


**Fig. 17.** Left: Influence of *Bi* on $K_{ig}$ for FTS and runaway. Right: Influence of *Bi* on ratio of $\Delta T_{bed,2D}$ to overall difference $T_{max} - T_{wall,2}$. Conditions of FTS and values of $T_{ig}$ as in Tab. 1 and Fig. 7.

Eq. (27) is graphically represented in Fig. 17 (left) and compared to the correlation shown in Fig. 8, which was empirically just derived by comparing the results of the 1D and 2D models. The agreement between both correlations is remarkably good. The influence of *Bi* on the ratio of the temperature difference within the bed to the overall difference is also highlighted in Fig. 17 (right).

For practical *Bi* values between 1 and 10, the ignition-related factor $K_{ig}$ varies between 7.1 and 5.5, with an average of 6.3 (Fig. 17, left). This is consistent with the constant value of 6.12, which has been recommended in the literature for predicting the onset of parametric sensitivity (Westerink et al., 1990; Crider and Foss, 1965). To illustrate the impact of $K_{ig}$ on reactor performance in a 1D model, selected results for temperatures and CO conversion are listed in Table 3 for different $K_{ig}$ values corresponding to practically relevant *Bi* numbers. For comparison, the constant literature value of 6.12 is also included. FTS was chosen as an instructive example.

First, the ignition temperature $T_{ig}$ (the highest cooling temperature $T_{cool}$ at which runaway is avoided) was determined. Then, a safe operating condition was modeled by assuming a cooling temperature $T_{safe}$ that is 5 K below $T_{ig}$. The results in Table 3 show significant differences: The CO conversion varies from 71 to 81 %, the ignition temperature $T_{ig}$ ranges from 223 to 231 °C, and the mean bed temperature $T_{mean}$ spans from 241 to 251 °C. These findings emphasize that assuming a constant $K_{ig}$ can lead to both under- and overestimation of reactor sensitivity. Even below ignition conditions, reactor performance parameters differ considerably, highlighting the necessity of a variable $K_{ig}$ approach in 1D modeling.

**Table 3**
CO conversion and characteristic temperatures derived by 1D model for different $K_{ig}$ values and $U_{th}$ based on Eq. (10). The minimum and maximum $K_{ig}$ values are related to practical *Bi* values ranging from 1 to 10. $T_{mean}$ refers to position of axial T-maximum.

| $K_{th}$ | $U_{th}$ (Eq. (10)) in W m$^{-1}$ K$^{-2}$ | $T_{cool} = T_{ig}$ in °C | $T_{cool} = T_{safe} = T_{ig} - 5$ K in °C | | |
|---|---|---|---|---|---|
| | | | $T_{cool}$ in °C | $T_{mean}$ in °C | $X_{CO}$ in % |
| 5.5 (*Bi* = 10, Eq. (27)) | 393 | 222.8 | 217.8 | 240.7 | 70.5 |
| 6.12[a] | 420 | 225.0 | 220.0 | 243.3 | 73.3 |
| 7.1 (*Bi* = 1, Eq. (27)) | 503 | 231.1 | 226.1 | 250.5 | 80.5 |

[a] Constant value of $K_{ig}$ recommended in the literature (see text) to predict onset of sensitivity.

At this point, we would like to note that, to the best of our knowledge, the calculation of the corrected radial temperature profile using the method described in Equations (18) to (22), or a similar approach, has not yet been published. Additionally, correlations such as Equation (23) and Equation (27) for determining the heat transfer parameters *K* and $K_{ig}$ as a function of *Bi*, *Ar*, or $\Delta T_{bed}$, among others, have also not been previously reported. This is particularly surprising, given the large number of publications – some of which are cited in this work – that have examined radial heat transport in cooled fixed-bed reactors as well as one-dimensional and two-dimensional reactor models. We therefore hope that our contribution is both novel and valuable.

### 4.2. Improved method to determine critical conditions of wall cooled fixed-bed reactors

The critical runaway conditions can be estimated using two dimensionless numbers, as introduced by Barkelew (1959). The first parameter is the cooling effectiveness number, given by

$$N_{cool} = \frac{U_{th}\frac{4}{d_{tube}}\Delta T_{ad}}{r_{m,CO,T_{cool}}\rho_{bed|\Delta_R H|E_A}} \tag{28}$$

With $r_{m,CO,Tcool}$ as reaction rate at $T_{cool}$. The second parameter is the adiabatic number, defined as

$$N_{ad} = \frac{E_A \Delta T_{ad}}{RT_{cool}^2} = Ar\Delta T_{ad} \tag{29}$$

which expresses the thermal sensitivity of the reaction. The ratio of these two parameters is frequently used for the analysis of thermal sensitivity, given by:

$$\frac{N_{cool}}{N_{ad}} = \frac{U_{th}\frac{4}{d_{tube}}RT_{cool}^2}{r_{m,CO,T_{cool}\rho_{bed}|\Delta_R H|E_A}} \tag{30}$$

For a cooled fixed-bed reactor, the maximum axial temperature occurs near the front part of the reactor. In the case of FTS with a tube length of

12 m, the axial position of this temperature maximum is around $z = 2$ m (see Fig. 4). This position is the critical location for runaway. Although reactant concentrations at the temperature maximum are lower than their initial values (for FTS, CO and $H_2$ concentrations are reduced), the sensitivity analysis for runaway behavior is based on the initial concentrations, meaning that $r_{m,CO,Tcool}$ is calculated using these values. The real decline in reactant concentrations, which reaches about 20 % for FTS, is approximated in the runaway diagram in Fig. 18 (left), which correlates $N_{cool}/N_{ad}$ and $N_{ad}$. This diagram was originally derived by Barkelew (1959) by inspecting a large number of numerical integrations of reactor systems before high-speed computing became available. Depending on the reaction order, critical conditions are reached when

$$\left(\frac{N_{cool}}{N_{ad}}\right)_{crit} = 2.72 - \frac{C}{\sqrt{N_{ad}}} \pm 0.15 \tag{31}$$

where $C = 0$ for a zero-order reaction ($n = 0$), $C = 2.6$ for $n = 0.5$, and $C = 3.37$ for $n = 1$, as described by Baerns et al. (2006) and Jess and Wasserscheid (2020). The curves in Fig. 18 (left) for different reaction orders define stability boundaries, separating the regions of stable and unstable operation regarding runaway. The uncertainty of $N_{cool}/N_{ad}$ is typically ± 0.15 (Baerns et al., 2006).

For FTS, the reaction order with respect to syngas concentration (CO + $H_2$) is approximately 0.5, and $N_{ad} = 34$ ($\Delta T_{ad,FTS} \approx 1000$ K). This means that thermal runaway should occur when

$$\left(\frac{N_{cool}}{N_{ad}}\right)_{crit,FTS} \leq 2.27 \pm 0.15 (\text{for} n = 0.5) \tag{32}$$

The value of $N_{cool}$ from Eq. (28) is directly proportional to the overall thermal transmittance $U_{th}$ and thus depends on the parameter $K$, as determined by Eq. (27). Additionally, $N_{cool}$ depends on the reciprocal of the reaction rate at $T_{cool}$, which decreases as $Bi$ increases (see Figs. 7 and 10).

If a constant value of $K = 8$ is incorrectly assumed, the critical term $N_{cool}/N_{ad}$ becomes significantly overestimated, as shown by the red data points in Fig. 18 (right). This overestimation leads to values much higher than the "real" value of 2.27 for FTS. Consequently, for $Bi > 1$, assuming $K = 8$ results in a huge overestimation of reactor stability with respect to runaway behavior, and the magnitude of this overestimation increases significantly for $Bi > 5$ (Fig. 18, right).

This effect arises because the heat transfer resistance of the bed $R_{bed}$ becomes increasingly dominant compared to the wall resistance $R_{wall}$. Assuming a constant $K = 8$ underestimates this effect quite strongly. However, when $K$ is adjusted according to Eq. (27), the critical term $N_{cool}/N_{ad}$ is correctly predicted to be near 2.27, as calculated by Eq. (30) and illustrated in Fig. 18 (right, blue data). It should be noted that the critical values of $N_{cool}/N_{ad}$ were calculated in both cases – for $K = 8$ and for $K = f(Bi)$ – based on the "true" critical cooling temperatures (ignition values) derived by the 2D model. This was done to explicitly illustrate the impact of $K$ and $Bi$ on the critical value of $N_{cool}/N_{ad}$.

To summarize: For analyzing thermal runaway using a 1D model, such as determining the critical cooling temperature or the maximum allowable tube diameter for a given cooling condition, Eq. (27) should be used to adjust the parameter $K$ and thus the value of $U_{th,1D}$ for the given Bi number.

An improved yet simple method is finally proposed in this work for determining the critical cooling (ignition) temperature $T_{ig}$ of wall-cooled fixed-bed reactors without requiring a full reactor model. This method requires knowledge of only four key parameters: the effective radial thermal conductivity $\lambda_{rad}$, the heat transfer coefficient at the wall $\alpha_{wall}$, the reaction rate $r_m$ at any value of $T_{cool}$ (and thus also $E_A$), and the reaction order $n$. These values can be estimated from heat transfer correlations and kinetic studies. Other required data – such as tube size, reaction enthalpy, adiabatic temperature rise, and catalyst bulk density – are typically well-known.

The suggested procedure to determine the ignition temperature $T_{ig}$ follows these steps:

1. Calculate $N_{ad}$ using Eq. (29) with the activation energy $E_A$, adiabatic temperature rise $\Delta T_{ad}$, and an initial estimate of the cooling temperature $T_{cool}$. If necessary, refine $N_{ad}$ iteratively.
2. Determine the critical value of $N_{cool}/N_{ad}$ for the given reaction order and $N_{ad}$ using Eq. (31).
3. For any Biot number, calculated by Eq. (11) along with the values of $\lambda_{rad}$, $\alpha_{wall}$, and $d_{tube}$, use Eq. (27) to obtain the appropriate value of $K_{ig}$ and then determine $U_{th}$ by Eq. (10).

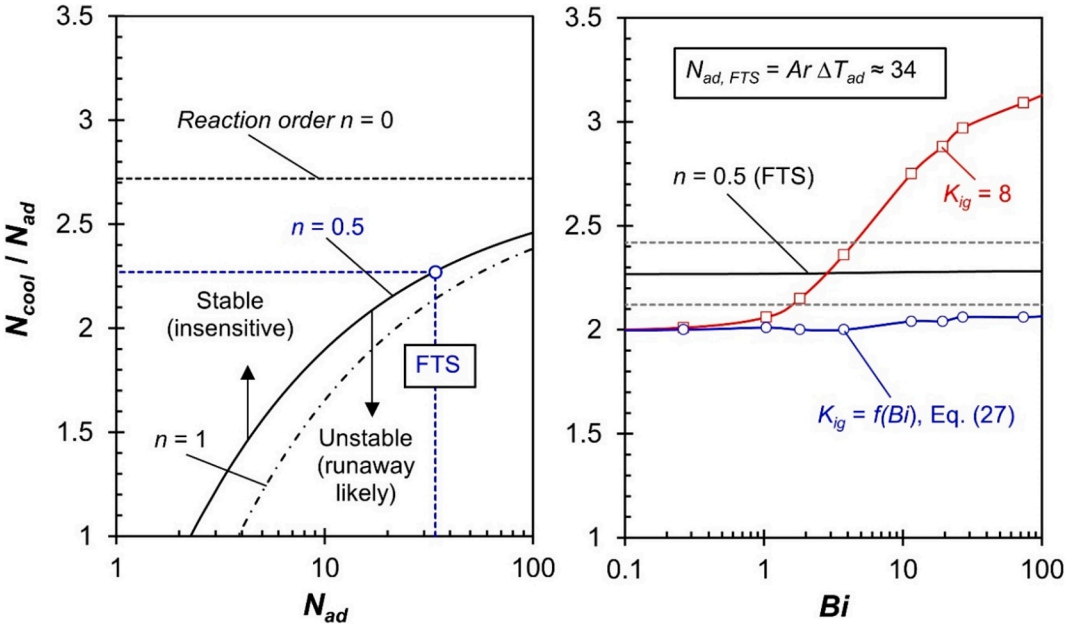


**Fig. 18.** Left: Runaway diagram for different reaction orders n according to Barkelew (1959) and Baerns et al. (2006). Right: Influence of Bi number on critical term $N_{cool}/N_{ad}$ with regard to ignition (Eq. (32)) for the conditions of FTS, i.e. $N_{ad} = Ar\ \Delta T_{ad} = 34$. Blue data points: Values with K = f(Bi) according to Eq. (27); red data: result for K = 8. The two dashed lines indicate margin of deviation of critical value of $N_{cool}/N_{ad}$ (Eq. (32)).

4. Adjust $T_{cool}$ iteratively until the calculated value of $N_{cool}/N_{ad}$ from Eq. (30) matches the critical value obtained from Eq. (31), ensuring that $T_{cool} = T_{ig}$.
5. Fig. 19 illustrates the ignition temperatures $T_{ig}$ calculated using this method for FTS ($E_A = 74$ kJ/mol and temperatures around 220 °C). The results obtained using $K = f(Bi)$ from Eq. (27) are shown as blue data points. For comparison, the ignition temperatures predicted using the incorrect assumption of a constant $K = 8$ (red data) and the value given by Westerink (1990) of $K = 6.12$ are also presented. Additionally, the "true" ignition temperatures obtained from the 2D model are included as black data.

The results clearly show that the suggested method with $K = f(Bi)$ closely matches the "true" ignition temperatures derived from the 2D model, with deviations of less than 4 K. In contrast, assuming $K = 6.12$ or $K = 8$ leads to deviations of up to 8 K or 10 K, respectively.

The small and systematic difference between the ignition temperatures derived using our method and the true 2D model values may stem from a potential weakness or inaccuracy in the correlations, Eq. (31) and Eq. (32), used to calculate the critical term $N_{cool}/N_{ad}$. For example, Barkelew (1959) used a value of $K = 8$ to calculate $U_{th}$ by Eq. (10), which yields a higher value of $N_{cool}$ (Eq. (28)) and of $N_{cool}/N_{ad}$ (Eq. (30)), respectively, compared to using a value of $K < 8$. This could be an indication that the critical value of $N_{cool}/N_{ad}$ according to Eq. (31) is a bit too high. Notably, if this term were 2.05 instead of 2.27, the calculated ignition temperatures would almost exactly match the 2D model values, see Fig. 18 (right), which indicates that this hypothesis could be correct.

More importantly, the 2D model predicts a strong decrease in $T_{ig}$ with increasing Biot number. For instance, within the practical range of $1 < Bi < 10$, the ignition temperature drops from 231 °C to 218 °C. This trend is only accurately captured by the proposed method using $K = f(Bi)$, whereas assuming a constant $K$ fails to account for this behavior correctly.

## 5. Conclusions and outlook

This study presents a refined approach for modeling heat transfer and thermal stability in wall-cooled fixed-bed reactors, with a focus on accurately predicting ignition conditions and the overall heat transfer coefficient $U_{th}$ in one-dimensional (1D) reactor models. The parameter $K$, which determines the temperature gradient present in the fixed-bed directly at the internal reactor wall, is thereby a crucial factor, needed to calculate $U_{th}$.

A key outcome is the development of new correlations for the factor $K$, which replaces the commonly used but oversimplified assumption of $K = 8$. The results demonstrate that:

For ignition conditions, where thermal sensitivity and runaway risk are high, $K_{ig}$ is solely a function of the Bi number (Eq. (27)). For $Bi < 1$, $K_{ig}$ approaches 8, while for $Bi > 10$, it converges toward 5.

For subcritical conditions, where cooling temperatures remain below the runaway threshold, $K$ is best determined by Eq. (23), which depends on the $Ar$ number and the normalized bed temperature difference $\Delta T_N$. This correlation ensures a more accurate estimation of $U_{th}$ than any fixed value of $K$.

These correlations were derived from a detailed comparison of 1D and 2D models, considering the impact of activation energy and radial temperature gradients on the effective heat transfer from bed to wall. A theoretical analysis of the influence of the reaction on the radial temperature profile in a fixed-bed was also conducted, which provides solid theoretical grounds for the presented results. While initially applied to Fischer-Tropsch synthesis, the approach is also in general valid for wall-cooled fixed-bed reactors.

A new method for predicting ignition conditions without relying on a reactor model is also introduced in this work. This method requires only two heat transfer parameters ($\lambda_{rad}$, $\alpha_{wall}$), typically calculated by literature correlations, and data on the reaction kinetics (rate $r_m$, $E_A$, and order $n$), mostly obtained from experimental data. The new correlations correctly predict the strong decrease in $T_{ig}$ with increasing $Bi$, an effect missed when using a constant $K$ in 1D models. The ignition temperatures obtained with the proposed method closely match the 2D model results (deviation < 4 K), whereas assuming $K = 6.1$ or 8, as recommended in the literature, leads to deviations of up to 10 K.

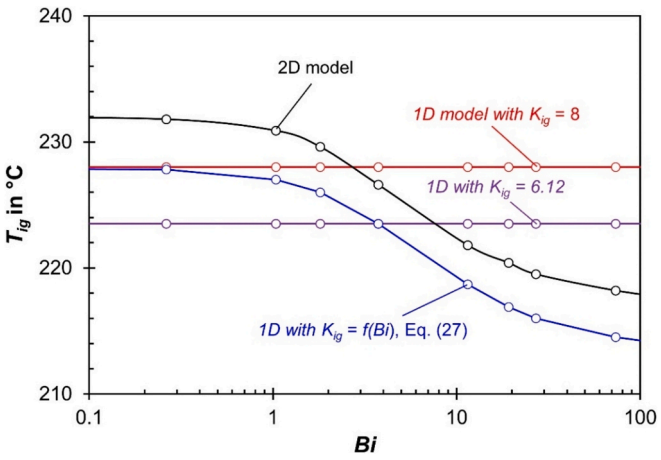


**Fig. 19.** Ignition temperatures (critical value of $T_{cool}$) of FTS calculated by Eq. (10), (11), (27), (29), (30), and (31) for $N_{cool}/N_{ad}$ of 2.27. Blue data: $U_{th}$ and $K = f(Bi)$ according to Eq. (27), i.e. for a range of 516 W m$^{-2}$ K$^{-1}$ ($Bi = 0.1$) to 338 W m$^{-2}$ K$^{-1}$ ($Bi = 100$). Red data: $U_{th}$ for $K = 8$ (516 W m$^{-2}$ K$^{-1}$); black data: result of 2D model ("true" benchmark values).

Future work will extend this analysis to reaction orders between zero and two and also evaluate alternative modeling approaches, such as the $\lambda_{rad}(r)$-model, which considers a radial variation of $\lambda_{rad}$ instead of a lumped heat transfer coefficient $\alpha_{wall}$. The improved modeling framework developed in this study provides a more accurate and computationally efficient approach for predicting reactor stability, offering significant value for industrial-scale reactor design and operation, particularly in highly exothermic reactions where thermal runaway must be controlled.

In conclusion, this work presents a robust framework for accurately predicting ignition conditions and thermal stability in wall-cooled fixed-bed reactors, ensuring both safe operation and optimal design.

Declaration of generative AI and AI-assisted technologies Statement

During the preparation of this work the authors used ChatGPT 4.0 in order to assist in drafting and refining the English text. After using this tool, the authors reviewed and edited the content as needed and take full responsibility for the content of the published article.

## CRediT authorship contribution statement

**Christoph Kern:** Software, Conceptualization. **Andreas Jess:** Writing – review & editing, Supervision, Project administration, Investigation, Formal analysis, Conceptualization.

## Declaration of competing interest

The authors declare that they have no known competing financial interests or personal relationships that could have appeared to influence the work reported in this paper.

## Data availability

Data will be made available on request.

## References


Baerns, M., Behr, A., Brehm, A., Gmehling, J., Hofmann, H., Onken, U., Renken, A., 2006. Technische Chemie. Wiley-VCH, Weinheim.

Barkelew, 1959. Stability of chemical reactors. Chem. Eng. Prog. Symp. Ser. 55, 37–46.

Bey, O., Eigenberger, 2001. Gas flow and heat transfer through catalyst filled tubes. Int. J. Therm. Sci. 40, 152–164.

Chao, R.E., Caban, R.A., Irizarry, M.M., 1973. Wall heat transfer to chemical reactors. Can. J. Chem. Eng. 51, 67–70.

Crider, J.E., Foss, A.S., 1965. Effective wall heat transfer coefficients and thermal resistances in mathematical models of packed beds. AIChE J. 11, 1012.

Dixon, A.G., Gurnon, A.K., Nijemeisland, M., Stitt, E.H., 2013. CFD testing of the pointwise use of the Zehner-Schlünder formulas for fixed-bed stagnnt thermal conductivity. Int. Comm. in Heat Mass Transfer 42, 1–4.

Dixon, A.G., 1996. An improved equation for the overall heat transfer coefficient in packed beds. Chem. Eng Processing 35, 323–331.

Emig, G., Klemm, E., 2005. Technische Chemie. Springer, Berlin.

Froment, G.F., Bischoff, K.B., 1990. Chemical Reactor Analysis and Design. John Wiley, New York.

Hofmann, H., 1979. Fortschritte bei der Modellierung von Festbettreaktoren. Chem. Ing. Tech. 51, 275.

Jess, A., Wasserscheid, P., 2020. Chemical Technology: From Principles to Processes, 2nd ed. Wiley, Weinheim, Germany.

Kern, C., Jess, A., 2009. Modelling of multi-tubular reactors for Fischer-Tropsch synthesis. Chem. Eng. Technol. 32 (8), 1164–1175.

Kern, C., Jess, A., 2023a. Performance of a multi-tubular Fischer-Tropsch reactor with two catalytic zones of different intrinsic chemical activity. Cat. Sci. Techn. 13, 516–527.

Kern, C., Jess, A., 2023b. Improvement of a multi-tubular Fischer-Tropsch reactor with gas recycle by appropriate combination of axial activity distribution and gas velocity. Cat. Sci. Techn. 13, 2212–2222.

Kern, C., Jess, A., 2023c. Significance of pressure drop, changing molar flow rate, and formation of steam in the accurate modeling of a multi-tubular Fischer-Tropsch reactor with cobalt as catalyst. Processes 11, 3281.

Kern, C., Jess, A., 2024a. Design and techno-economic analysis of Fischer-Tropsch fixed-bed synthesis with cobalt as catalyst. Energy Techn. 2301534.

Kern, C., Jess, A., 2024b. On the role of radial dispersion in the behavior of a cooled fixed-bed reactor: Simulation of Fischer-Tropsch synthesis with a cobalt-based catalyst. Chem Eng. Techn., e202400201

Li, C.-H., Finlayson, B.A., 1977. Heat transfer in packed beds - a reevaluation. Chem. End. Sci. 32, 1055–1066.

Mendez, C.I., Ancheyta, J., Trejo, F., 2017. Modeling of catalytic fixed-bed reactors for fuels production by fischer-tropsch synthesis. Energy Fuels 31, 13011–13042.

Mendez, C.I., Ancheyta, J., 2019a. Dynamic one-dimensional pseudohomogeneous model for Fischer-Tropsch fixed-bed reactors. Fuel 252, 371–392.

Mendez, C.I., Ancheyta, J., Trejo, F., 2019b. Importance of proper hydrodynamics modelling in fixed-bed reactors: Fischer-Tropsch synthesis study case. Can. J. of Chem. Eng. 97, 2685–2698.

Mendez, C.I., Ancheyta, J., 2020a. Kinetic models for Fischer-Tropsch synthesis for the production of clean fuels. Cat. Today 353, 3–16.

Mendez, C.I., Ancheyta, J., 2020b. Modeling and control of Fischer-Tropsch synthesis fixed-bed reactor with a novel mechanistic kinetic approach. Chem. Eng. J. 390, 124489.

Mendez, C.I., Ancheyta, J., Trejo, F., 2022. On the use of steady-state optimal initial operating conditions for control scheme of a fixed-bed Fischer-Tropsch reactor. Arabian J. for Science and Eng. 47, 6099–6113.

Pöhlmann, F., Jess, A., 2016a. Influence of syngas composition on the kinetics of Fischer-Tropsch synthesis with Cobalt as catalyst. Energy Technol. 4 (2016), 55–64.

Pöhlmann, F., Jess, A., 2016b. Interplay of reaction and pore diffusion during cobalt-catalyzed Fischer-Tropsch Synthesis with $CO_2$-rich syngas. Cat. Today 275 (2016), 172–182.

Pöhlmann, F., Rössler, S., Kern, C., Jess, A., 2016. Accumulation of liquid hydrocarbons in catalyst pores during Co-catalyzed Fischer-Tropsch synthesis. Cat. Sci. Techn. 6 (2016), 6593–6604.

Rößler, S., Kern, C., Jess, A., 2018. Formation and vaporization of hydrocarbons during cobalt-catalysed Fischer-Tropsch synthesis. Chem. Ing. Techn. 90 (2018), 634–642.

Pöhlmann, F., 2017. Zusammenspiel von chemischer Reaktion und Porendiffusion bei der kobaltkatalysierten Fischer-Tropsch-Synthese unter Einsatz von $CO_2$-haltigem Synthesegas, Ph.D. Thesis, University Bayreuth, Germany.

Sanchez-Lopez, J.R.G., Martinez-Hernandez, A., Hernandez-Ramitez, A., 2017. Modeling of transport phenomena in fixed-bed reactors for the Fischer-Tropsch reaction: a brief literature review. Rev. Chem. Eng. 33 (2), 109.

Sauerhöfer-Rodrigo, F., Díaz, I., Rodríguez, M., Pérez, 2024. Modelling of fixed-bed and slurry bubble column reactors for Fischer–Tropsch synthesis. Rev. Chem. Eng, 151–192.

Tsotsas, E., Schlünder, E.U., 1990. Heat transfer in packed beds with fluid flow: Remarks on the meaning and calculation of a heat transfer coefficent at the wall. Chem. Eng. Sci. 45, 819–937.

Vortmeyer, D., Haidegger, E., 1991. Discrimination of three approaches to evaluate heat fluxes for wall-cooled fixed-bed chemical reactors. Chem. Eng. Sci. 46, 2651–2660.

Westerterp, K.R., van Swaaij, W.P.M., Beenackers, A.A.C.M., 1998. Chemical Reactor Design and Operation. John Wiley & Sons, New York.

Westerink, E.J., Koster, N., Westerterp, K.R., 1990. The choice between cooled tubular reactor models: Analysis of the hot-spot. Chem. Eng. Sci. 45, 3343–3455.

Wilson, K.B., 1946. Calculation and analysis of longitudinal temperature gradients in tubular reactors. Trans. Inst. Chem. Engrs. 24, 77–83.

Winterberg, M., Tsotsas, E., Krischke, A., Vortmeyer, D., 2000. A simple and coherent set of coefficients for modelling of heat and mass transport with and without chemical reaction in tubes filled with spheres. Chem. Eng. Sci. 55, 967–979.

Winterberg, M., Tsotsas, E., 2000. Modelling of heat transport in packed beds with spherical particles for various bed geometries and/or thermal boundary conditions. Int. J. Therm. Sci. 39, 556–570.

Zenner, A., Fiaty, K., Belliere-Baca, V., Rocha, C., Gauthier, G., Edouard, D., 2019. Effective heat transfers in packed bed: Experimental and model investigation. Chem. End. Sci. 201, 424–436.